UCLA
COMPUTATIONAL AND APPLIED MATHEMATICS

Kinetic Theory for Bubbly Flow I: Collisionless Case

Giovanni Russo
Peter Smereka

April 1993

CAM Report 93-07

Department of Mathematics
University of California, Los Angeles
Los Angeles, CA. 90024-1555

Kinetic Theory for Bubbly Flow I: Collisionless Case

Giovanni Russo [1]
Dipartimento di Matematica Pura ed Applicata
Università dell'Aquila, Italy
and
Peter Smereka [2]
Department of Mathematics
University of California, Los Angeles CA 90024-1555

ABSTRACT

A kinetic theory for incompressible dilute bubbly flow is presented. The Hamiltonian formulation for a collection of bubbles is outlined. A Vlasov equation is derived for the one-particle distribution function with a self-consistent field starting with the Liouville equation for the N-particle distribution function and using the point-bubble approximation. A stability condition which depends on the variance of the bubbles momenta and the void fraction is derived. If the variance is small then the linearized initial-value problem is ill-posed. If it is sufficiently large, then the initial value problem is well-posed and a phenomenon similar to Landau damping is observed. The ill-posedness is found to be the result of an unstable eigenvalue, whereas the Landau damping arises from a resonance pole. Numerical simulations of the Vlasov equation in 1-D are performed using a particle method. Some evidence of clustering is observed for initial data with small variance in momentum.

[1] Research supported in part by a grant # DAAL03-91-G-0162 from the Army Research Office

[2] Research supported in part by the National Science Foundation through a postdoctoral fellowship and the Army Research Office, grant # DAAL03-91-G-0162

1 Introduction

Bubbly flows appear in many physical systems, such as pipes in chemical plants or nuclear reactors. One of the main objectives of research in this field is the derivation of effective equations that describe the bulk behavior of such systems. A typical procedure consists of taking space or ensemble averages of the bubble distribution. The system of conservation laws is then closed by constitutive relations.

Bubbly flows can be quite complex and much work has therefore been focused on dilute, inviscid, irrotational flows with massless bubbles (which we shall call an ideal bubbly flow). There are two reasons for this: first, it represents a good approximation of some physical systems (for example, void wave propagation of millimeter-sized air bubbles in water) and second, it is mathematically much simpler than the case where viscosity, compressibility and turbulence can play a role. The main physical process present in ideal bubbly flows is momentum exchange between the bubbles and the liquid, the so-called virtual mass effect.

Despite the restriction to ideal bubbly flows, there is little agreement in the literature on the form these effective equations should take (see, for example, Wallis [1] or the recent discussion between van Wijngaarden [2] and Geurst [3]). The main source of disagreement arises from the choice of constitutive laws used to close the system. It is most common to spatially average the fluid equations and close the system using results concerning single bubble motion in an arbitrary flow. Biesheuvel & van Wijngaarden [4], Drew & Wood [5], Lhuillier [6] and Pauchon & Banerjee [7], amongst others, have derived effective equations in this manner for bubbly flow.

Other approaches have also been used; van Beek [8] obtained effective equations by ensemble averaging, and Geurst [9] derived effective equations by volume averaging the energy; he then used a variational principle with the volume averaged energy as the Lagrangian. Wallis [1], Pauchon & Smereka [10], and Smereka & Milton [11] have made several observations concerning Geurst's equations.

A kinetic approach has been used by Biesheuvel & Gorissen [14] and van Wijngaarden & Kapteyn [15] to study void waves in bubble flows. Biesheuvel

& Gorissen start with a conservation law for an N-particle distribution function. They derive effective equations by taking moments of the distribution function. They are forced, however, to close their system using physical intuition. They obtain results similar to those found by Batchelor [16] in his study of fluidized beds. van Wijngaarden & Kapteyn considered a suspension of bubbles using pair-wise interactions. They focused their study on steady traveling waves and performed experiments which were found to be in reasonably good agreement with their theory.

More recently, Sangani & Didwania [12] and Smereka [13] performed numerical simulations of bubbles in a periodic box where the box contained an inviscid and irrotational liquid. In both studies it was found that when the bubbles were given similar velocities, they would tend to form clusters similar to the ellipsoidal clusters suggested in [11]. One of us [13], however, found that if the variance in bubbles' velocities was sufficiently large the clustering was inhibited. Both studies also found that the addition of gravity and liquid viscosity would result in pancake-shaped clusters for large time.

In this paper we give a kinetic formulation of rarefied bubbly flow. We derive an equation for the density function analogous to the Vlasov equation for plasma. Closer analogies can be found, however, in the work of Liboff [30] who used a Vlasov equation to study gas-liquid condensation, and in works about a kinetic description of a gas of vortex dipoles [31, 32]. The Hamiltonian formulation that we derive has some analogies with the Hamiltonian formulation of incompressible fluid dynamics [33, 34].

We consider a set of identical bubbles in an incompressible, irrotational liquid. The bubbles are considered incompressible. There are regimes in which this model is a good approximation of an actual physical system. We neglect collisions; their effect will be considered in a following paper. We neglect the effect of viscosity and gravity, because we are interested in describing the collective effects due to the interaction with the fluid. As we shall see, this interaction will give rise to a Hamiltonian system for N interacting particles. The Hamiltonian structure will be the basis for the derivation of a kinetic description of the flow. The effect of gravity and viscosity could be added later to the model. The main result of the paper is the derivation of a Vlasov equation for the density of bubbles in phase space, $f(\boldsymbol{x}, \boldsymbol{p}, t)$.

The Vlasov equation with a self consistent field describes collective behavior of a large number of particles subject to long range interactions. Typical

examples are given in plasma physics and in astrophysics. In the first case the interaction is a Coulomb force, and in the second it is given by Newton's gravitational law [36, 35]. In both cases the force decays as $1/r^2$ (in the plasma case it is repulsive, while in the gravitational case it is attractive).

As we shall see, in the case of dilute bubbly flow the interaction is given by a dipole field. In spite of the fact that this interaction decays faster than the Coulomb force ($1/r^3$), still it may be considered long-range, and collective behavior due to the mutual interactions of the bubbles can be observed.

One of the main points of this paper consists in the derivation of a kinetic theory for particles that have a dipole interaction. In this respect the interest of the paper is not confined to people working in bubbly flow.

The plan of the paper is as follows. In the next section we consider the problem of the motion of a set of N identical bubbles in an inviscid, incompressible, irrotational fluid. We derive a Lagrangian that describes the dynamics of the system with $3N$ degrees of freedom. We write then the Hamiltonian formulation for the motion of the N bubbles. The Lagrangian and the Hamiltonian of the system are complicated functions that can be computed only by solving a Laplace equation for the stream function. In Section 3 we make use of the point-bubble approximation; that is formally based on an asymptotic expansion in terms of the void fraction. This gives us a simple approximation for the Hamiltonian of the system.

In Section 4 we derive the Vlasov equation for bubbly flow, starting from the Liouville equation associated to the Hamiltonian flow. We then make use of the BBGKY hierarchy and the assumption of molecular chaos to write the Vlasov equation for the density function in phase space. An expression is given for the coefficients of the Vlasov equation as functionals of the distribution function.

In Section 5 we perform a linear analysis of the kinetic equation. We find that the well-posedness of the initial value problem for the linearized equation depends on the relation between the void fraction and the variance in momenta of the bubbles. If the variance is large enough, the linear modes are damped. This effect closely resembles Landau damping found in a plasma [17]. If the variance is small the initial value problem is ill-posed. In Section 6 we will present some numerical results that use a particle-in-cell method. In the unstable case the bubbles tend to cluster; this is in agreement with other results in the literature [12], [13].

2 Hamiltonian Formulation

We will consider a collection of rigid, massless bubbles of identical size that are initially at rest in an inviscid, incompressible, and quiescent liquid in three dimensions. The dominant physical effects that we ignore are gravity and liquid viscosity. We plan to add those effects in a future model.

We shall use bold-faced characters to denote 3-D vectors. The bubbles are impulsively set into motion, thereby giving rise to an irrotational flow. The velocity of the liquid, $\boldsymbol{v}_\ell$, is therefore the gradient of a velocity potential, ϕ, hence,

$$\boldsymbol{v}_\ell = \nabla\phi, \quad \boldsymbol{x} \in \mathcal{V},$$

where $\mathcal{V}$ is the domain occupied by the liquid. The velocity potential satisfies the following elliptic problem:

$$\nabla^2\phi = 0, \quad \boldsymbol{x} \in \mathcal{V}, \tag{1}$$

with boundary conditions on the bubble surfaces being,

$$\frac{\partial\phi}{\partial n} = \boldsymbol{u}_k \cdot \boldsymbol{n}, \quad \boldsymbol{x} \in S_k,\ k = 1, \ldots, N, \tag{2}$$

where $\boldsymbol{n}$ is the outward drawn normal from the liquid surface, $\boldsymbol{u}_k$ is the velocity of the k-th bubble and S_k is the surface of bubble k. The condition at infinity is

$$\nabla\phi = 0, \tag{3}$$

which corresponds to the zero volumetric flux frame of reference. Because Eqs. (1), (2) and (3) are linear in ϕ, we can write

$$\phi = \sum_{k=1}^{N} \boldsymbol{u}_k \cdot \boldsymbol{\psi}_k, \tag{4}$$

where $\boldsymbol{\psi}_k$ is a vector valued function that depends only on the positions of the bubbles. The boundary conditions are then satisfied by taking

$$\frac{\partial\boldsymbol{\psi}_k}{\partial n} = \begin{cases} \boldsymbol{n} & \text{on the } k\text{-th bubble} \\ 0 & \text{on the other bubbles.} \end{cases}$$

In order to write the Hamiltonian of the system we need to find the kinetic energy. The total energy of the system is entirely contained in the liquid since the bubbles have no mass. It is given by

$$T = \frac{1}{2}\rho_\ell \int_\nu |\nabla\phi|^2 d\boldsymbol{x}, \tag{5}$$

where ρ_ℓ is the density of the liquid. This expression can be written in an alternate form using Green's Theorem:

$$T = \frac{\rho_\ell}{2} \sum_{k=1}^{N} \int_{S_k} \phi \frac{\partial\phi}{\partial n} dS. \tag{6}$$

The contribution to the energy at infinity vanishes by virtue of (3). We substitute (4) into (6) to obtain

$$T = \frac{1}{2}\rho_\ell \sum_{k=1}^{N} \int_{S_k} \left(\sum_i \boldsymbol{u}_i \cdot \boldsymbol{\psi}_i \right) \boldsymbol{u}_k \cdot \boldsymbol{n}\, dS_k,$$

which can be written as

$$T = \frac{1}{2} \sum_{i,j} \boldsymbol{u}_i^T A_{ij} \boldsymbol{u}_j, \tag{7}$$

where

$$A_{ij} = \rho_\ell \int_{S_j} \boldsymbol{\psi}_i \boldsymbol{n}^T dS_j. \tag{8}$$

It is shown [13] that the matrices A_{ij} satisfy

$$A_{ij} = A_{ji}$$

and

$$A_{ij} = A_{ij}^T.$$

It follows from the definition of $\boldsymbol{\psi}_i$ and from (8) that A_{ij} depends only on the positions of the bubbles, therefore

$$A_{ij} = A_{ij}(\boldsymbol{x}_1, \ldots, \boldsymbol{x}_N),$$

and the kinetic energy T is the Lagrangian of a system of $3N$ degrees of freedom with coordinates $\{\boldsymbol{x}_1, \ldots, \boldsymbol{x}_N\}$ and velocities $\{\boldsymbol{u}_1, \ldots, \boldsymbol{u}_N\}$. The

equations of motion are consequently given by the Euler-Lagrange equations; the generalized momenta are given by

$$\boldsymbol{p}_k = \frac{\partial T}{\partial \boldsymbol{u}_k} = \sum_j A_{kj} \boldsymbol{u}_j. \tag{9}$$

Substituting (8) into (9), we obtain

$$\boldsymbol{p}_k = \rho_\ell \int_{S_k} \phi \, \boldsymbol{n} \, dS_k,$$

which is the well-known expression for the impulse associated to the k-th bubble. To write this system in Hamiltonian form, we solve (9) for $\boldsymbol{u}_k$ in terms of $\boldsymbol{p}_k$, to obtain

$$\boldsymbol{u}_k = \sum_j B_{kj} \boldsymbol{p}_j, \tag{10}$$

with

$$\sum_k A_{ik} B_{kj} = I \delta_{ij}, \tag{11}$$

where I is the 3×3 identity matrix and δ_{ij} is the Kronecker delta. Equation (11) can always be solved for B_{ij} because it can be written in the form

$$\mathcal{A}\mathcal{B} = \mathcal{I}, \tag{12}$$

where $\mathcal{I}$ is the $3N \times 3N$ identity matrix,

$$\mathcal{A} = \begin{pmatrix} A_{11} & \cdots & A_{1N} \\ \vdots & \cdots & \vdots \\ A_{N1} & \cdots & A_{NN} \end{pmatrix},$$

and $\mathcal{B}$ is similarly defined. It follows from (5) and (7) that $\mathcal{A}$ must be positive definite and therefore invertible; hence $\mathcal{B}$ is well defined. We substitute (10) into (7) to obtain the Hamiltonian of the system:

$$H = \frac{1}{2} \sum_{i,j} \boldsymbol{p}_i^T B_{ij} \boldsymbol{p}_j.$$

The equations of motion are therefore

$$\begin{aligned} \dot{\boldsymbol{x}}_k &= \frac{\partial H}{\partial \boldsymbol{p}_k} = \sum_i B_{ki} \boldsymbol{p}_i, \\ \dot{\boldsymbol{p}}_k &= -\frac{\partial H}{\partial \boldsymbol{x}_k} = -\frac{1}{2} \sum_{ij} \boldsymbol{p}_i^T \frac{\partial B_{ij}}{\partial \boldsymbol{x}_k} \boldsymbol{p}_k. \end{aligned} \tag{13}$$

The starting point of the kinetic theory is Liouville's equation for the N-particle distribution function associated to the Hamiltonian system (13), $f^{(N)}(\boldsymbol{x}_1, \ldots, \boldsymbol{x}_N, \boldsymbol{p}_1 \ldots, \boldsymbol{p}_N, t)$. It is given by

$$\frac{\partial f^{(N)}}{\partial t} + \sum_k \left[\boldsymbol{u}_k \cdot \frac{\partial f^{(N)}}{\partial \boldsymbol{x}_k} + \boldsymbol{F}_k \cdot \frac{\partial f^{(N)}}{\partial \boldsymbol{p}_k} \right] = 0, \tag{14}$$

where

$$\begin{aligned} \boldsymbol{u}_k &= \frac{\partial H}{\partial \boldsymbol{p}_k}, \\ \boldsymbol{F}_k &= -\frac{\partial H}{\partial \boldsymbol{x}_k}. \end{aligned} \tag{15}$$

An inspection of (10) reveals that $\dot{\boldsymbol{x}}_k$ is not simply proportional to $\boldsymbol{p}_k$ as in gas dynamics. For this reason, it is not equivalent to choose the momentum or the velocity as an independent coordinate in the derivation of this kinetic theory. A similar lack of proportionality also appears in other physical systems. In semiconductors, for example, the velocity is a function of the wave vector. The wave vector is used as an independent variable in the kinetic description [19].

3 Point-Bubble Approximation

There is no simple analytic expression for $\mathcal{A}$ and $\mathcal{B}$ for a generic distribution of bubbles. Here we will make use of the *point-bubble approximation.* In this approximation the contribution of a single bubble to the velocity potential is given by a dipole field. This dipole field is an exact solution for a single bubble moving in an unbounded fluid. For the case of two bubbles this approximation is valid to $O((a/r_{12})^6)$, where a is the bubble radius and r_{12} is the distance between the bubbles [20]. The point-bubble approximation for $\mathcal{A}$ [13], is:

$$A_{ij} = \begin{cases} \rho_\ell \dfrac{\tau}{2} I & i = j \\ \rho_\ell \dfrac{3\tau}{4} \left(\dfrac{a}{|r_{ij}|} \right)^3 \left(I - 3 \dfrac{r_{ij} r_{ij}^T}{|r_{ij}|^2} \right) & i \neq j \end{cases}, \tag{16}$$

where τ is the bubble volume and $\boldsymbol{r}_{ij} = \boldsymbol{x}_i - \boldsymbol{x}_j$.

Formally we can expect (16) to provide a good approximation as long as the bubbles are well-separated. Nevertheless, using a result due to Basset [21], it has been shown [13] that (16) provides a very accurate approximation even when the bubbles collide. Therefore we expect (16) to give a good approximation for dilute bubbly mixture even in presence of some clustering.

In recent work Kim & Prosperetti [22] and Sangani & Didwania [12] present schemes for an accurate numerical simulation of the motion of massless rigid spheres in a potential flow. These schemes can be used in connection with our theory for three different purposes: i) as a check of the validity of the point-bubble approximation, by comparing the field computed by an accurate numerical solution with the field due to a family of dipoles; ii) as a test for our theory (predictions of our theory can be compared to an accurate numerical simulation using a large number of bubbles); iii) as a guideline for the development of a kinetic theory that is valid for denser bubbly flows.

By inserting (16) into (12), we obtain, to the same order of approximation, the following expression for B_{ij}:

$$B_{ij} = \begin{cases} \dfrac{2}{\rho_\ell \tau} I & i = j \\ -\dfrac{3}{\rho_\ell \tau}\left(\dfrac{a}{|\boldsymbol{r}_{ij}|}\right)^3 \left(I - 3\dfrac{\boldsymbol{r}_{ij}\boldsymbol{r}_{ij}^T}{|\boldsymbol{r}_{ij}|^2}\right) & i \neq j \end{cases} . \tag{17}$$

In the analysis that follows it is useful to note that the Hamiltonian and the force can be written as

$$H = \frac{1}{2}\sum_k \boldsymbol{p}_k \cdot \boldsymbol{u}_k,$$

and

$$\dot{\boldsymbol{p}}_k = \boldsymbol{F}_k = -\frac{1}{2}\frac{\partial}{\partial \boldsymbol{x}_k}\sum_i \boldsymbol{p}_i \cdot \boldsymbol{u}_i, \tag{18}$$

where $\boldsymbol{u}_k$ is given by (10). Let us consider the term

$$\frac{\partial \boldsymbol{u}_i}{\partial \boldsymbol{x}_k} = \frac{\partial}{\partial \boldsymbol{x}_k}\sum_j B_{ij}\boldsymbol{p}_j$$

which, by virtue of (17), can be written as

$$\frac{\partial \boldsymbol{u}_i}{\partial \boldsymbol{x}_k} = \left(\frac{\partial}{\partial \boldsymbol{x}_i} \sum_j B_{ij} \boldsymbol{p}_j \right) \delta_{ik} + \frac{\partial}{\partial \boldsymbol{x}_k} B_{ik} \boldsymbol{p}_k. \tag{19}$$

Upon substituting (19) into (18), we find

$$\dot{\boldsymbol{p}}_k = \boldsymbol{F}_k = \sum_{j \neq k} \boldsymbol{F}_{kj}, \tag{20}$$

where

$$\boldsymbol{F}_{kj} = -\frac{\partial}{\partial \boldsymbol{x}_k} (\boldsymbol{p}_k^T B_{kj} \boldsymbol{p}_j). \tag{21}$$

The velocity of the k-th bubble can be written as

$$\boldsymbol{u}_k = \frac{2}{\tau \rho_\ell} \boldsymbol{p}_k + \sum_{j \neq k} \boldsymbol{u}_{kj}, \tag{22}$$

with

$$\boldsymbol{u}_{kj} = B_{kj} \boldsymbol{p}_j. \tag{23}$$

It should be noted that both $\boldsymbol{F}_{kj}$ and $\boldsymbol{u}_{kj}$ depend only on $\boldsymbol{p}_k, \boldsymbol{p}_j$ and $(\boldsymbol{x}_k - \boldsymbol{x}_j)$. By using (22), Eq. (20) can be written as follows:

$$\boldsymbol{F}_k = -\frac{\partial}{\partial \boldsymbol{x}_k} (\boldsymbol{p}_k \cdot \boldsymbol{u}_k). \tag{24}$$

Eq. (22) has the following interpretation: $\boldsymbol{u}_{kj}$ is proportional to the contribution to the liquid velocity at the center of the k-th bubble due the j-th bubble. It follows from [13] (see Eq. 3.29) that (22) can be written as

$$\boldsymbol{u}_k = \frac{2}{\tau \rho_\ell} \boldsymbol{p}_k + 3 \boldsymbol{v}_k^\infty, \tag{25}$$

where $\boldsymbol{v}_k^\infty$ is the so-called *ambient velocity* of the liquid at $\boldsymbol{x}_k$.

4 Vlasov Equation for Bubbly Flow

In this section we derive a self-consistent Vlasov equation for bubbles interacting via a dipole field. We start from the Liouville equation for the N-particle distribution function. We then make use of the BBGKY hierarchy to derive a self-consistent Vlasov equation for the one-particle density function in phase space. For convenience, the BBGKY hierarchy is closed by the assumption of molecular chaos.

For a description of the BBGKY hierarchy and the approximations entailed in the Vlasov equation see, for example, Chapman & Cowling [23] or Liboff [24]. In those cases the Vlasov equation is derived for particles interacting with a Coulomb field. Our case is quite different, since the particles interact with a dipole field which decays faster and is more singular at the origin. In spite of the faster decaying rate, however, the field may still be considered long-range, and collective behavior are described in terms of a self-consistent mean-field associated to the Vlasov equation.

We begin by writing the Liouville equation (14) in the form

$$\frac{\partial f^{(N)}}{\partial t} + \sum_k \left[\frac{\partial}{\partial \boldsymbol{x}_k} \cdot (\boldsymbol{u}_k f^{(N)}) + \frac{\partial}{\partial \boldsymbol{p}_k} \cdot (\boldsymbol{F}_k f^{(N)}) \right] = 0, \tag{26}$$

This is possible because of Hamilton's equations (15). Integrating the Liouville equation over

$$d\Omega_1 \equiv d\boldsymbol{x}_2 \cdots d\boldsymbol{x}_N \; d\boldsymbol{p}_2 \cdots d\boldsymbol{p}_N,$$

we obtain

$$\frac{\partial f^{(1)}}{\partial t} + \int \boldsymbol{u}_1 \cdot \frac{\partial f^{(N)}}{\partial \boldsymbol{x}_1} d\Omega_1 + \int \boldsymbol{F}_1 \cdot \frac{\partial f^{(N)}}{\partial \boldsymbol{p}_1} d\Omega_1 = 0, \tag{27}$$

where

$$f^{(1)}(\boldsymbol{x}_1, \boldsymbol{p}_1, t) = \int f^{(N)}(\boldsymbol{x}_1 \ldots \boldsymbol{x}_N, \boldsymbol{p}_1 \ldots \boldsymbol{p}_N, t)\, d\Omega_1$$

is the one-particle distribution function. Using equations (20), (22) and (24) for $\boldsymbol{u}_1$ and $\boldsymbol{F}_1$ in (27) we obtain

$$\frac{\partial f^{(1)}}{\partial t} + \frac{2}{\tau \rho_\ell} \boldsymbol{p}_1 \cdot \frac{\partial f^{(1)}}{\partial \boldsymbol{x}_1} + \sum_{k=2}^{N} \int \left(\boldsymbol{u}_{1k} \cdot \frac{\partial f^{(N)}}{\partial \boldsymbol{x}_1} + \boldsymbol{F}_{1k} \cdot \frac{\partial f^{(N)}}{\partial \boldsymbol{p}_1} \right) d\Omega_1 = 0.$$

By using the indistinguishability of particles $(2,\ldots,N)$ and the fact that $\boldsymbol{u}_{ik}$ and $\boldsymbol{F}_{ik}$ depend only on $\boldsymbol{x}_i, \boldsymbol{x}_k, \boldsymbol{p}_i$, and $\boldsymbol{p}_k$, we write the above equation as

$$\frac{\partial f^{(1)}}{\partial t} + \frac{2}{\tau\rho_\ell}\boldsymbol{p}_1 \cdot \frac{\partial f^{(1)}}{\partial \boldsymbol{x}_1} + (N-1)\int \left(\boldsymbol{u}_{12}\cdot\frac{\partial f^{(2)}}{\partial \boldsymbol{x}_1} + \boldsymbol{F}_{12}\cdot\frac{\partial f^{(2)}}{\partial \boldsymbol{p}_1}\right) d\boldsymbol{x}_2 d\boldsymbol{p}_2 = 0, \tag{28}$$

where

$$f^{(2)}(\boldsymbol{x}_1,\boldsymbol{x}_2,\boldsymbol{p}_1,\boldsymbol{p}_2,t) = \int f^{(N)}(\boldsymbol{x}_2,\ldots,\boldsymbol{x}_N,\boldsymbol{p}_1,\ldots,\boldsymbol{p}_N,t)\, d\boldsymbol{x}_3,\ldots,d\boldsymbol{x}_N, d\boldsymbol{p}_3,\ldots,d\boldsymbol{p}_N$$

is the two-particle distribution function. We write the two-particle distribution function as

$$f^{(2)}(\boldsymbol{x}_1,\boldsymbol{x}_2,\boldsymbol{p}_1,\boldsymbol{p}_2,t) = f^{(1)}(\boldsymbol{x}_1,\boldsymbol{p}_1,t) f^{(1)}(\boldsymbol{x}_2,\boldsymbol{p}_2,t) + c_2. \tag{29}$$

where c_2 is a measure of the correlation between bubbles 1 and 2. When $c_2 = 0$ then the bubbles are uncorrelated and we have molecular chaos.

Here the assumption of molecular chaos was used for convenience. We believe that it is not strictly necessary and that a rigorous mathematical derivation of the Vlasov equation can be obtained under more general assumptions, in the so called mean-field limit, as is done, for example, in the case of plasma [28]. Such a rigorous treatment, however, is beyond the scope of our analysis, and may be the subject of further research.

We substitute the expression (29) with $c_2 = 0$ in equation (28) to obtain

$$\frac{\partial f^{(1)}}{\partial t} + \left[\frac{2}{\tau\rho_\ell}\boldsymbol{p}_1 + (N-1)\left(\int \boldsymbol{u}_{12} f^{(1)}(\boldsymbol{x}_2,\boldsymbol{p}_2,t) d\boldsymbol{x}_2 d\boldsymbol{p}_2\right)\right]\cdot\frac{\partial f^{(1)}}{\partial \boldsymbol{x}_1}$$

$$+(N-1)\left(\int \boldsymbol{F}_{12} f^{(1)}(\boldsymbol{x}_2,\boldsymbol{p}_2,t) d\boldsymbol{x}_2 d\boldsymbol{p}_2\right)\cdot\frac{\partial f^{(1)}}{\partial \boldsymbol{p}_1} = 0.$$

It is convenient to use the density function in phase space,

$$f(\boldsymbol{x},\boldsymbol{p},t) = N f^{(1)}(\boldsymbol{x},\boldsymbol{p},t), \tag{30}$$

which has the property

$$\int f(\boldsymbol{x},\boldsymbol{p},t)d\boldsymbol{p} = n(\boldsymbol{x},t),$$

where $n(\boldsymbol{x},t)$ is the number of bubbles per unit volume. For large N the equation for $f(\boldsymbol{x},\boldsymbol{p},t)$ is

$$\frac{\partial f}{\partial t} + \boldsymbol{u}_1 \cdot \frac{\partial f}{\partial \boldsymbol{x}_1} + \boldsymbol{F}_1 \cdot \frac{\partial f}{\partial \boldsymbol{p}_1} = 0, \tag{31}$$

where

$$\boldsymbol{u}_1(\boldsymbol{x}_1,\boldsymbol{p}_1,t) = \frac{2}{\tau\rho_\ell}\boldsymbol{p}_1 + \int \boldsymbol{u}_{12}(\boldsymbol{x}_1,\boldsymbol{p}_1,\boldsymbol{x}_2,\boldsymbol{p}_2,t)f(\boldsymbol{x}_2,\boldsymbol{p}_2,t)d\boldsymbol{x}_2 d\boldsymbol{p}_2, \tag{32}$$

$$\boldsymbol{F}_1(\boldsymbol{x}_1,\boldsymbol{p}_1,t) = \int \boldsymbol{F}_{12}(\boldsymbol{x}_1,\boldsymbol{p}_1,\boldsymbol{x}_2,\boldsymbol{p}_2,t)f(\boldsymbol{x}_2,\boldsymbol{p}_2,t)d\boldsymbol{x}_2 d\boldsymbol{p}_2. \tag{33}$$

In order to evaluate the integrals contained in (32) and (33), we make use of expressions (21) and (23) which we rewrite here:

$$\boldsymbol{u}_{12} = B_{12}\boldsymbol{p}_2, \tag{34}$$

$$\boldsymbol{F}_{12} = -\boldsymbol{p}_1\frac{\partial B_{12}}{\partial \boldsymbol{x}_1}\boldsymbol{p}_2 = -\frac{\partial}{\partial \boldsymbol{x}_1}(\boldsymbol{p}_1 \cdot \boldsymbol{u}_{12}). \tag{35}$$

From (17), it follows that

$$B_{12}^{\alpha\beta} = \frac{9}{4\rho_\ell\pi}\frac{\partial^2}{\partial r_{12}^\alpha \partial r_{12}^\beta}\frac{1}{|\boldsymbol{r}_{12}|},$$

where $\alpha,\beta = 1,2$, and 3 denote the cartesian components. From (32), (34), and (35), the expression for $\boldsymbol{F}_1$ can be written as follows:

$$\boldsymbol{F}_1 = -\frac{\partial}{\partial \boldsymbol{x}_1}(\boldsymbol{p}_1 \cdot \boldsymbol{u}_1).$$

To develop the expression for $\boldsymbol{u}_1$, it is useful to introduce the momentum density:

$$\boldsymbol{j}(\boldsymbol{x}_2,t) = \int \boldsymbol{p}_2 f(\boldsymbol{x}_2,\boldsymbol{p}_2,t)\, d\boldsymbol{p}_2.$$

Then (32) and (33) become

$$u_1^\alpha = \frac{2}{\tau\rho_\ell} p_1^\alpha - \frac{9}{\rho_\ell} J^\alpha(x_1, t), \tag{36}$$

and

$$F_1^\alpha = p_1^\beta \frac{\partial}{\partial x_1^\alpha} J^\beta(x_1, t), \tag{37}$$

where

$$J^\alpha(x_1, t) = -\frac{1}{4\pi} \int \frac{\partial^2}{\partial x_1^\alpha \partial x_1^\beta} \frac{j^\beta(x_2, t)}{|x_1 - x_2|} dx_2. \tag{38}$$

(Here and in the sequel, we assume summation over repeated Greek indices). The integral in (38) is the continuous limit of the sum in Eq. (22). It represents the field created by a dipole distribution.

The velocity field generated by one bubble decays as $1/r^3$, and the force between two bubbles decays as $1/r^4$. This does not preclude the possibility of the force having a mean field description which is clear from (37). A mean field description can be expected under general circumstances, however. This point was made by Vlasov ([29], pg. 19) who argued that a mean field description was necessary whenever one wishes to capture collective behavior.

Liboff [30] made this point clear in his work on phase transitions. He considered an interaction force that decays as $1/r^n$ with $n = 2, 3, 4, \ldots$ and showed that there was collective behavior for all finite n. In the limit $n \to \infty$ the collective behavior disappears.

In what follows we shall develop a mean field description for (36) and (37). The integrand of (38) has a nonintegrable singularity and the integral is therefore taken as a principle value integral. This corresponds to the exclusion of all the bubbles within some small spherical volume around the bubble at x_1. In dielectric theory this corresponds to the Lorentz sphere. Therefore, the principle value of (38) corresponds to its mean field and we write

$$J = J_{mean} + J_{local} \tag{39}$$

where

$$J^\alpha_{mean}(x_1, t) = -\lim_{\epsilon \to 0} \frac{1}{4\pi} \int_{|x_1 - x_2| > \epsilon} \frac{\partial^2}{\partial x_1^\alpha \partial x_1^\beta} \frac{j^\beta(x_2, t)}{|x_1 - x_2|} dx_2. \tag{40}$$

and $\boldsymbol{J}_{local}$ is the contribution of the bubbles within the Lorentz sphere.

In Appendix A we prove that

$$\boldsymbol{J}_{mean}(\boldsymbol{x}_1,t) = \tilde{\boldsymbol{J}}(\boldsymbol{x}_1,t) - \frac{1}{3}\boldsymbol{j}(\boldsymbol{x}_1,t), \tag{41}$$

where

$$\tilde{J}^{\alpha}(\boldsymbol{x}_1,t) \equiv \frac{\partial^2}{\partial x_1^{\alpha}\partial x_1^{\beta}} \int G(\boldsymbol{x}_1,\boldsymbol{x}_2) j^{\beta}(\boldsymbol{x}_2,t) d\boldsymbol{x}_2, \tag{42}$$

and

$$G(\boldsymbol{x}_1,\boldsymbol{x}_2) \equiv -\frac{1}{4\pi|\boldsymbol{x}_1-\boldsymbol{x}_2|}$$

is Green's function of the Laplacian. In dielectric theory $\tilde{\boldsymbol{J}}$ corresponds to the macroscopic electric field and (41) is known as the Lorentz relation. A discussion of these matters can be found in a textbook of electromagnetic theory, see for example Reitz & Milford ([26], pgs. 68–96). As a result, the equation for $\boldsymbol{u}_1$ becomes

$$\rho_\ell \boldsymbol{u}_1 = \frac{2}{\tau}\boldsymbol{p}_1 - 9\tilde{\boldsymbol{J}}(\boldsymbol{x}_1,t) + 3\boldsymbol{j}(\boldsymbol{x}_1,t) - 9\boldsymbol{J}_{local}.$$

Substituting the expression for $\boldsymbol{J}$ into (37) combined with (31) gives

$$\frac{\partial f}{\partial t} + \boldsymbol{u}\cdot\frac{\partial f}{\partial \boldsymbol{x}} + \boldsymbol{F}\cdot\frac{\partial f}{\partial \boldsymbol{p}} = \left(\frac{\partial f}{\partial t}\right)_{local}, \tag{43}$$

with

$$\rho_\ell \boldsymbol{u} = \frac{2}{\tau}\boldsymbol{p} - 9\boldsymbol{J}_{mean} \tag{44}$$

and

$$\boldsymbol{F} = -\nabla(\boldsymbol{p}\cdot\boldsymbol{u}) \tag{45}$$

where the expressions for $\boldsymbol{u}$ and $\boldsymbol{F}$ now contain only the mean field contribution of $\boldsymbol{J}$. The right hand side of (43) takes into account the local effects, which are the short range forces experienced by the bubbles inside the Lorentz sphere. In addition to the dipole force between bubbles (and possible higher order terms), actual bubble collisions are also contained in this term. The effects of collisions are small when the Knudsen number, κ, given by

$$\kappa = \frac{\text{mean free path}}{\text{macroscopic length scale}}$$

is large. For bubbly fluids we do not know the Knudsen number *a priori* so we will consider two limits: $\kappa \to \infty$, which corresponds to the collisionless case and $\kappa \to 0$, which corresponds to the fluid dynamic limit. For the rest of this paper we shall focus on the case $\kappa \to \infty$ so we assume

$$\left(\frac{\partial f}{\partial t}\right)_{local} = \left(\frac{\partial f}{\partial t}\right)_{collisions} = 0$$

Just to see the order of magnitude of a possible Knudsen number, we consider a typical case. A simple analysis shows that the Knudsen number is given by $\kappa = (4/3)a/(L\varepsilon_0)$, where a is the bubble radius, L is the macroscopic length scale (for example, the wavelength of a void wave), and ε_0 is the void fraction. In the case where the bubbles have a radius of 1 mm with $L = 1$ to 10 cm and the void fraction is $\varepsilon_0 = 0.01$, it would be in the range $\kappa \approx 1$ to 10.

To derive the self consistent field we introduce a potential, Φ, that satisfies

$$\Delta\Phi = \nabla \cdot \boldsymbol{j},$$

and we write Eq. (42) as

$$\tilde{\boldsymbol{J}} = \nabla\Phi.$$

We observe that

$$\begin{aligned} \nabla \times \tilde{\boldsymbol{J}} &= 0, \\ \nabla \cdot \tilde{\boldsymbol{J}} &= \nabla \cdot \boldsymbol{j}, \end{aligned}$$

therefore the vector $\tilde{\boldsymbol{J}}$ is the projection of $\boldsymbol{j}$ into the space of curl-free vectors. In summary, the Vlasov equation for an ideal bubbly fluid with a self consistent field is given by

$$\frac{\partial f}{\partial t} + \boldsymbol{u} \cdot \frac{\partial f}{\partial \boldsymbol{x}} + \boldsymbol{F} \cdot \frac{\partial f}{\partial \boldsymbol{p}} = 0 \tag{46}$$

with

$$\rho_\ell \boldsymbol{u} = \frac{2}{\tau}\boldsymbol{p} - 3(3\nabla\Phi - \boldsymbol{j}), \tag{47}$$

and

$$\begin{aligned} \boldsymbol{F} &= -\nabla(\boldsymbol{p} \cdot \boldsymbol{u}), \\ \Delta\Phi &= \nabla \cdot \boldsymbol{j}, \\ \boldsymbol{j} &= \int \boldsymbol{p} f \, d\boldsymbol{p}. \end{aligned} \tag{48}$$

As in the discrete case (see Eq. 25), the second term on the right-hand side of equation (47) is proportional to the ambient liquid velocity, i.e.:

$$v^{\infty} = -\frac{1}{\rho_\ell}(3\nabla\Phi - j).$$

Notice that the vector field, $j(x,t)$, is not necessarily irrotational, in spite of the fact that the original liquid flow is irrotational.

In one dimension the Vlasov equation reduces to

$$\frac{\partial f}{\partial t} + u\frac{\partial f}{\partial x} + F\frac{\partial f}{\partial p} = 0, \tag{49}$$

$$\begin{aligned} \rho_\ell u &= \frac{2}{\tau}p - 6j, \\ F &= \frac{6p}{\rho_\ell}\frac{\partial j}{\partial x}, \\ j &= \int pf\,dp, \end{aligned} \tag{50}$$

where $f(x,p,t) = \int f(x,y,z,p,p_y,p_z,t)dp_y dp_z$ is assumed to be independent of y and z. The ambient liquid velocity is

$$v^{\infty} = -\frac{2}{\rho_\ell}j. \tag{51}$$

We make a remark about the validity of a kinetic model. The kinetic approach can give a good quantitative description of the behavior of the bubbles only if the total number of bubbles is large enough. By considering a typical macroscopic size of the bubble channel (a few meters long and a fraction of a meter wide), some typical bubble radius (of the order of a millimeter) and a void fraction of about 1%, one can check that we are in a region where a one-particle distribution function can provide a meaningful description (see Ref. [27], pg. 19).

5 Linear Analysis in One-Space Dimension

In this section we study the stability of the Vlasov equation linearized about a spatially homogeneous stationary solution. We shall prove that the stability

depends on the void fraction and the spreading in momentum of the bubble distribution. If the spreading is large enough, the initial value problem for the linear Vlasov equation is well-posed, otherwise it is ill-posed. In the well-posed region we observe an effect similar to the Landau damping for the Vlasov-Poisson system in plasma physics.

We consider the one-dimensional Vlasov equation (49), and observe that any time independent, spatially homogeneous density function, $f_0(p)$, is a solution of Eq. (49). We shall now write the equations in nondimensional form (the nondimensional variables are denoted by an asterisk). The independent variables are

$$p = \frac{\tau \rho_\ell u_0}{2} p^*, \quad x = L\, x^*, \quad t = \frac{L}{u_0}\, t^*, \tag{52}$$

and the dependent variables are

$$\begin{aligned} j(x,t) &= \frac{\tau \rho_\ell u_0}{2L^3} j^*(x^*, t^*), \\ f(x,p,t) &= \left(\frac{2}{\tau \rho_\ell u_0 L^3}\right) f^*(x^*, p^*, t^*). \end{aligned}$$

We choose the length scale to be $L^3 = \tau$, and the velocity u_0, so that

$$n_0 \frac{\tau \rho_\ell u_0}{2} = n_0 p_0 \equiv \int p f_0(p) dp,$$

where $n_0 \equiv \int f_0(p)\, dp$. With the nondimensional variables, Eqs. (49–50) become

$$\begin{gathered} \frac{\partial f}{\partial t} + (p - 3j)\frac{\partial f}{\partial x} + 3p \frac{\partial j}{\partial x}\frac{\partial f}{\partial p} = 0, \\ j(x,t) = \int p f(x,p) dp, \end{gathered} \tag{53}$$

where the asterisks have been dropped. The linearized equation for $f_1 = f - f_0$ is

$$\frac{\partial f_1}{\partial t} + (p - 3j_0)\frac{\partial f_1}{\partial x} + 3p \frac{\partial j_1}{\partial x}\frac{\partial f_0}{\partial p} = 0, \tag{54}$$

where

$$j_1(x,t) = \int f_1(x,p,t) p\, dp, \quad j_0 = \int f_0(p) p\, dp.$$

We take the Fourier transform in space, and the Laplace transform in time of $f_1(x,p,t)$ to obtain

$$sF_1 - \hat{f}_1(k,p,0) + ik(p-3j_0)F_1 + 3pikJ_1\frac{\partial f_0}{\partial p} = 0, \tag{55}$$

where

$$F_1(k,p,s) = \int_{-\infty}^{+\infty} dx \int_0^{+\infty} dt\, e^{-st-ikx} f_1(x,p,t),$$

and $J_1 = J_1(k,s)$ is analogously defined. $\hat{f}_1(k,p,0)$ is the Fourier transform of the initial perturbation. We solve (55) for F_1 and obtain

$$F_1 = \frac{1}{s+ik(p-3j_0)}\left[\hat{f}_1(k,p,0) - 3ikJ_1(k,s)p\frac{\partial f_0(p)}{\partial p}\right]. \tag{56}$$

We multiply by p, integrate both sides of the above equation and solve for J_1 to obtain

$$J_1 = \frac{\frac{1}{ik}\int_{-\infty}^{+\infty} \frac{\hat{f}_1(k,p,0)p\,dp}{p-\lambda}}{1+3\int_{-\infty}^{+\infty} \frac{p^2}{p-\lambda}\frac{\partial f_0}{\partial p}dp}, \tag{57}$$

where $\lambda = 3j_0 + is/k$.

Let $\hat{j}_1(k,t)$ be the Fourier transform of $j_1(x,t)$. Its time evolution is determined by taking the inverse Laplace transform of J_1. Formally $J_1(k,s)$ is defined only for $\mathrm{Re}(s) > 0$ $(\mathrm{Im}(\lambda) > 0)$ by computing the integrals that appear in (57) along the real axis. Following Landau's analysis, we perform analytical continuation for $\mathrm{Re}(s) < 0$ $(\mathrm{Im}(\lambda) < 0)$ using the path shown in Figure 1.

Next, we consider spatial homogeneous solutions of Eq. (49), $f_0(p)$, that have the following properties:

1. $f_0(p)$ is either an entire function of p or has a finite number of poles, none of which is on the real axis.

2. $f_0(p)$ is a unimodal distribution symmetric around its mean.

If the mean of $f_0(p)$ is nonzero, we scale p so that the mean is unity. We shall denote by σ^2 the variance of the distribution $f_0(p)$, hence

$$\varepsilon_0\sigma^2 = \int (p-1)^2 f_0(p)dp,$$

where

$$\varepsilon_0 = \int f_0(p)dp.$$

Let us consider the expression (57) for J_1. We shall consider initial perturbations, $f_1(x,p,0)$, which are either entire functions of p or are of the form $f_1(x,p,0) = \varphi(x)f_0(p)$. From the assumptions on $f_0(p)$ and $f_1(x,p,0)$, it follows that the poles of the numerator are also poles of the denominator; therefore, the poles of J_1 are given by the zeroes of the denominator. The denominator of (57) is denoted as $\mathcal{H}(\lambda)$:

$$\mathcal{H}(\lambda) = 1 + 3\int_{-\infty}^{\infty} \frac{p^2}{p-\lambda}\frac{\partial f_0}{\partial p}(p)dp. \tag{58}$$

Let λ_m denote a generic root of $\mathcal{H}(\lambda) = 0$ and λ_M the root with the greatest imaginary part. The poles of J_1 are then located, in the complex s-plane, at

$$s_m = -ik(\lambda_m - 3j_0). \tag{59}$$

The long time behavior of $\hat{j}_1$ is determined by $s_M = -ik(\lambda_M - 3j_0)$, since this is the pole with the largest real part. If $\mathrm{Re}(s_M) < 0$ then $\hat{j}_1$ will decay to zero exponentially. This decay is analogous to Landau damping in a plasma [17]. If $\mathrm{Re}(s_M) > 0$ then $\hat{j}_1$ grows exponentially. It is evident from (59) that the growth rate is proportional to k indicating that the initial value problem is ill-posed.

The behavior of $\hat{f}_1$ can be obtained from Eq. (56). In addition to the poles present in (57), F_1 has a pole on the imaginary axis located at

$$s_q = ik(3j_0 - p).$$

This indicates that when $\mathrm{Re}(s_M) < 0$, the long time behavior of $\hat{f}_1(x,p,t)$ will be

$$\hat{f}_1(k,p,t) \approx \exp[ik(3j_0 - p)t],$$

and when $\mathrm{Re}(s_M) > 0$ then

$$\hat{f}_1(k,p,t) \approx \exp[ik(3j_0 - \lambda_M - p)t].$$

5.1 Transition curve

The transition between the stable and unstable regimes given by $\mathrm{Re}(s_M) = 0$, is equivalent to

$$\mathrm{Im}(\lambda_M) = \max_j \ \mathrm{Im}(\lambda_j) = 0. \tag{60}$$

The solution $f(x,p,t) = f_0(p)$ is stable if

$$\mathrm{Im}(\lambda_M) < 0.$$

The λ_j's are functions of ε_0 and σ, therefore (60) represents a curve in the $\varepsilon_0 - \sigma$ plane. In this section, we shall derive an expression for this curve of the form

$$\sigma = \sigma_L(\varepsilon_0).$$

We recall that the integral in (58) is taken along the real axis when $\mathrm{Im}(\lambda) > 0$ and along the path shown in Figure 1 when $\mathrm{Im}(\lambda < 0)$. Equation (58) is rewritten as

$$\mathcal{H}(\lambda) = 1 + 3\int_{-\infty}^{\infty} \frac{p^2(p-\lambda_R)}{(p-\lambda_R)^2+\lambda_I^2}\frac{\partial f_0}{\partial p}dp$$
$$+3i\lambda_I \int_{-\infty}^{\infty} \frac{p^2}{(p-\lambda_R)^2+\lambda_I^2}\frac{\partial f_0}{\partial p}dp,$$

where $\lambda = \lambda_R + i\lambda_I$. We are interested in roots with zero imaginary part and therefore take the limit as $\lambda_I \to 0$ of $\mathcal{H}(\lambda)$. We observe that for any continuous real function, $\varphi(x)$,

$$\lim_{\xi\to 0}\frac{1}{\pi}\int \frac{\xi}{x^2+\xi^2}\varphi(x)\,dx = \varphi(0)$$

i.e. $\xi/(\pi(x^2+\xi^2))$ converges to the Dirac delta function as $\xi \to 0$; we obtain

$$\lim_{\lambda_I\to 0^+} \mathcal{H}(\lambda) = 1 + 3\int_{-\infty}^{\infty}\frac{p^2}{p-\lambda_R}\frac{\partial f_0}{\partial p}dp + 3i\pi\lambda_R^2\frac{\partial f_0}{\partial p}(\lambda_R)$$

where the integration is along the real axis. Setting $\mathcal{H}(\lambda) = 0$ implies

$$1 + 3\int_{-\infty}^{\infty}\frac{p^2}{p-\lambda_R}\frac{\partial f_0}{\partial p}dp = 0, \tag{61}$$

$$\lambda_R^2\frac{\partial f_0}{\partial p}(\lambda_R) = 0. \tag{62}$$

Equation (62) has two solutions, namely $\lambda_R = 0$ and $\lambda_R = 1$ ($\lambda_R = 1$ is a solution because f_0 has a maximum at 1). For $\lambda_R = 0$, Eq. (61) will be satisfied only if $\varepsilon_0 = 1/3$, which is well outside the validity of our model; consequently, we will not consider this case further. Note that, in view of our hypothesis, the integrand of the above equation is a smooth function.

By virtue of the second hypothesis on $f_0(p)$ assumed in the previous section, we can write

$$f_0(p) = \frac{\varepsilon_0}{\sigma} g\left(\frac{p-1}{\sigma}\right), \tag{63}$$

where $g(x)$ has zero mean and unit variance. Substituting (63) into (61), we obtain the relation

$$\sigma_L = \sqrt{\frac{3\varepsilon_0 I}{1-3\varepsilon_0}}, \tag{64}$$

where

$$I = -\int_{-\infty}^{\infty} \frac{g'(x)}{x} dx > 0. \tag{65}$$

To summarize, we have shown that when $\sigma = \sigma_L(\varepsilon_0)$, $\lambda = 1$ is a root of $\mathcal{H}(\lambda) = 0$. In other words, (64) is a curve in the $\sigma - \varepsilon_0$ plane in which a root of $\mathcal{H}(\lambda) = 0$ has zero imaginary part. To prove that (64) is the transition curve we must prove that there are no other roots of $\mathcal{H}(\lambda) = 0$ with $\mathrm{Im}(\lambda) > 0$ when $\sigma = \sigma_L(\varepsilon_0)$. This is achieved with the theorem below which is proved in Appendix B.

Theorem. *The equation $\mathcal{H}(\lambda; \varepsilon_0, \sigma) = 0$ with $\varepsilon_0 < 1/3$ has only one root with $Im(\lambda) > 0$ when $\sigma < \sigma_L(\varepsilon_0)$, and has no root with $Im(\lambda) > 0$ when $\sigma > \sigma_L(\varepsilon_0)$.*

In view of (59) this theorem shows that if $\sigma > \sigma_L(\varepsilon_0)$, the initial value problem for the linearized equation is well-posed and if $\sigma < \sigma_L(\varepsilon_0)$ it is ill-posed. In Appendix C it is shown that a resonance pole arising from the analytic continuation of the resolvent is responsible for the Landau damping and when $\sigma < \sigma_L$ the resonance pole becomes an unstable eigenvalue.

Example. If the spatially homogeneous distribution is a Gaussian, then

$$g(x) = \frac{1}{\sqrt{2\pi}} \exp\left(-\frac{x^2}{2}\right)$$

and therefore

$$\sigma_L = \sqrt{\frac{3\varepsilon_0}{1-3\varepsilon_0}}.$$

We also mention that Sangani & Didwania [18] have also examined the stability of homogeneous bubble arrangements by computing the gradient of dispersed phase stress tensor with respect to the void fraction. They found that this quantity was negative in a number of circumstances indicating an instability. In these cases the bubbles were given identical velocities, therefore the variance of the momentum is small and their observation of instability is consistent with the results of this section.

Finally, we observe that our theory, and in particular the results of the stability analysis, were developed under the assumption that viscous effects are negligible. We expect that a model that takes into account the viscosity would have similar stability properties (in particular, that the some linear modes will be amplified if the variance in momentum distribution is small enough), provided the viscous time scale is much larger than the time scale of the instability.

5.2 An explicit solution

We construct an explicit solution to Equation (54). We consider the following spatially homogeneous distribution:

$$f_0 = \frac{2\varepsilon_0\sigma^3}{\pi(\sigma^2+(p-1)^2)^2}, \tag{66}$$

which has the properties

$$\int f_0 dp = \varepsilon_0,$$
$$\int p f_0 dp = \varepsilon_0,$$
$$\int (p-1)^2 f_0 dp = \varepsilon_0\sigma^2.$$

To compute the transition curve corresponding to the stationary solution (66), we note that

$$g(x) = \frac{2}{\pi}\frac{1}{(1+x^2)^2},$$

and therefore,

$$\sigma_L = 3\sqrt{\frac{\varepsilon_0}{1-3\varepsilon_0}}.$$

Next we consider an initial perturbation of the form

$$f_1(x,p,0) = \varphi(x)f_0(p).$$

The integrands that appear in (57) now have three poles given by

$$p = \lambda, \quad 1 \pm i\sigma,$$

and no poles at infinity. This means that the integral along the real axis ($\mathrm{Im}(\lambda) > 0$) or the path shown in Figure 1 ($\mathrm{Im}(\lambda) < 0$) is always given by

$$2\pi i[a_1 + a_2],$$

where a_1 and a_2 are the residues of the integrand at $p = \lambda$ and $p = 1 + i\sigma$. After a simple calculation, we find

$$J_1 = -i\varepsilon_0\hat{\varphi}(k)\frac{(s-ikA)(s-ikB)}{\Pi_{j=1}^{3}(s-ik\omega_j)}, \tag{67}$$

where $\hat{f}_1(k,p,0) = \hat{\varphi}(k)f_0(p)$, $A = 3j_0 - 1 + \sigma^2 + 2i\sigma$, $B = 3j_0 - 1 + i\sigma$, and $\omega_j = 3j_0 - \lambda_j$. The λ_j's are the roots of the following polynomial:

$$\begin{aligned} P(\lambda) &= \lambda^3 - 3\lambda^2(1 - 2\varepsilon_0 - i\sigma) \\ &\quad +3\lambda(1-3\varepsilon_0)(1-i\sigma)^2 - (1-3\varepsilon_0)(1-i\sigma)^3. \end{aligned}$$

The inverse Laplace transform of (67) is

$$\hat{j}_1 = \varepsilon_0\hat{\phi}(k)\sum_{\ell=1}^{3} a_\ell \exp(ik\omega_\ell t)$$

where

$$a_\ell = \frac{\omega_\ell^2 - (A+B)\omega_\ell + AB}{(\omega_\ell - \omega_n)(\omega_\ell - \omega_m)},$$

and $(\ell,\ m,\ n)$ is a cyclic permutation of $(1,2,3)$. The time evolution of j_1 is given by the inverse Fourier transform, therefore

$$j_1(x,t) = \frac{1}{2\pi}\int_{-\infty}^{\infty} dk\, \hat{j}_1(k,t)e^{ikx}. \tag{68}$$

We shall make use of this formula later when comparing the results of linear analysis with numerical computations.

6 Numerical simulation

In this section we show some numerical solutions of the one-dimensional Vlasov equation (49–50). We use a particle-in-cell method, which is quite standard for equations of this type [35, 36]. We consider the initial value problem for the one dimensional Vlasov equation (53):

$$\begin{aligned} \frac{\partial f}{\partial t} + (p - 3j)\frac{\partial f}{\partial x} + 3p\frac{\partial j}{\partial x}\frac{\partial f}{\partial p} &= 0, \\ j(x,t) = \int p f(x,p,t) dp, & \\ f(x,p,0) = f_0(x,p). & \end{aligned} \tag{69}$$

We use periodic boundary conditions in x with period L. The density function $f(x,p,t)$ is approximated by a set of equally weighted particles:

$$f(x,p,t) \approx f_N(x,p,t) = \frac{\varepsilon_0 L}{N} \sum_{i=1}^{N} \delta(x - x_i(t))\, \delta(p - p_i(t)), \tag{70}$$

where ε_0 is the mean void fraction. The space is divided into N_c cells of size $H = L/N_c$. The flux, j, is computed at the center of the cell and stored in the vector J using the following weighting:

$$\mathrm{J} = \frac{N_c}{N} \sum_{i=1}^{N} p_i \Lambda\left(\frac{x_i - X_k}{H}\right),$$

where $X_k = (k - 1/2)H$ is the center of cell k, and

$$\Lambda(x) = \begin{cases} |1 - x| & \text{if } |x| \le 1 \\ 0 & \text{if } |x| > 1 \end{cases}$$

is the "tent function" [36]. The vector JX containing the derivatives of $j(x)$ is obtained by centered differencing:

$$\mathrm{JX}_k = \frac{\mathrm{J}_{k+1} - \mathrm{J}_{k-1}}{2H}, \quad k = 1, \ldots, N_c.$$

where $\mathrm{J}_{N+1} \equiv \mathrm{J}_1$ and $\mathrm{J}_0 \equiv \mathrm{J}_N$. The particles satisfy the equations of motion:

$$\begin{aligned} \dot{x}_i &= u_i, \\ \dot{p}_i &= F_i, \end{aligned} \tag{71}$$

with $u_i = p_i - 3\,\mathrm{FNJ}(x_i)$ and $F_i = 3\,p_i\,\mathrm{FNJX}(x_i)$. The functions FNJ and FNJX are obtained by interpolation using the same function in the weighting step, hence

$$\begin{aligned} \mathrm{FNJ}(x) &= \sum_{k=1}^{N_c} \mathrm{J}_k \Lambda\left(\frac{x - X_k}{H}\right), \\ \mathrm{FNJX}(x) &= \sum_{k=1}^{N_c} \mathrm{JX}_k \Lambda\left(\frac{x - X_k}{H}\right). \end{aligned}$$

The equations of motion are then solved by a forward-Euler scheme.

In order to complete the description of the scheme, we have to specify how to approximate the initial conditions (i.e., how to determine the initial position and momentum of the particles). One possibility would be to extract N random points in phase space with probability distribution proportional to $f_0(x,p)$. This procedure, however, would introduce undesired and unnecessary statistical fluctuations. To avoid this problem, the initial condition is chosen in such a way so that the discrete measure (70) is a good approximation of the continuous measure (69). This is achieved in the following two steps:

Step 1. Approximate the uniform distribution in the unit square with N points, $\{(\xi_i, \eta_i),\ i = 1, \ldots, N\}$. The quality of the approximation can be measured by the so-called *discrepancy* between the two measures. There are several sequences for which the bound in the discrepancy is close to the optimal one. We used the van der Corput sequence in our calculations. For more details on the subject, see, for example, Refs. [37] and [38].

Step 2. Consider a mapping $T : [0, L] \times I\!R \to I\!R^2$, from phase space to the unit square, whose Jacobian is the function $f_0(x,p)$. This will map a measure with density $f_0(x,p)$ into the Lebesgue measure in the unit square. An example of such a mapping is given by:

$$\xi = T_1(x) = \frac{\int_0^x dx' \int_{-\infty}^{+\infty} dp\, f_0(x',p)}{\int_0^L dx' \int_{-\infty}^{+\infty} dp\, f_0(x',p)},$$

$$\eta = T_2(x,p) = \frac{\int_{-\infty}^{p} dp' f_0(x,p')}{\int_{-\infty}^{+\infty} dp' f_0(x,p')}.$$

If $f_0(x,p) > 0$ this mapping is invertible. Let $T^{-1} : [0,1]^2 \to I\!R^2$ denote the inverse mapping; then the initial conditions are obtained from

$$(x_i^0, p_i^0) = T^{-1}(\xi_i, \eta_i), \quad i = 1, \ldots, N.$$

It is possible to show that in an appropriate metric space the distance between the discrete and the continuous measure satisfy the following bound:

$$d(f_0, f_N) \leq CV(f_0)\frac{\log N}{N},$$

where C is a constant of order unity and $V(\cdot)$ denotes the variation of a function [38].

Numerical results

We present the results for a few runs of the numerical scheme just outlined, in both the stable and unstable regimes. We consider an initial distribution of the form:

$$f(x,p,0) = \varepsilon_0 \left(1 + \alpha \sin\left(\frac{2\pi x}{L}\right)\right) f_0(p),$$

with $f_0(p)$ given by (66). In the first run we choose $\varepsilon_0 = 0.01, \sigma = 0.5$ and $\alpha = 0.6$ (this is in the well-posed regime). The results are reported in Figures 2 and 3. Figure 2 shows a sample of 2,000 particles in phase space for different times. Figure 3 shows the momentum flux, $j(x,t)$, for the same times. The circles are the result of the particle code and the continuous line represents the exact solution of the linearized equations, Eq. (68). The parameters used in the computation are $L = 100, N_c = 20$, and $N = 65,535$. The time step is $\Delta t = 0.1$ and the output time interval is $\Delta t_{\text{out}} = 80$. The agreement between the linear theory and the numerical results is good even if the initial amplitude of the perturbation is not small.

In the second run, we choose $\varepsilon_0 = 0.01, \sigma = 0.2$, and $\alpha = 0.1$. (this is in the ill-posed regime). All the other parameters are the same as in the previous case. The plot of the points in phase space is shown in Figure 4, and the value of the flux is reported in Figure 5. The continuous line is the result of linear theory and the circles represent the numerical result. The agreement with linear theory is good for short times; the nonlinear effects then start to be relevant.

As a last example, we consider a case in the strongly ill-posed region. We take $\sigma = 0.1$ and $\alpha = 0.4$. The results of the calculation are reported in Figures 6 and 7. The ill-posedness develops into oscillations which grow very rapidly, but after a long time a single spike in the density propagates in the fluid. This effect is numerical evidence of bubble clustering. The size of the clustered region decreases when the variance σ^2 gets smaller. This result is in qualitative agreement with numerical simulations obtained by Sangani & Didwania [12] and Smereka [13].

7 Conclusions

In this paper, a kinetic theory for an ideal bubbly liquid has been formulated. The main ingredients of this theory are the Hamiltonian equations of motion, the point-bubble approximation, and the use of a Vlasov approach to reduce the N-particle distribution function to a one-particle distribution function. The approach neglects the local interactions of the bubbles; these are included in the sequel to this paper. Any spatially homogeneous distribution function is a solution of our Vlasov equation for bubbly flow. It was demonstrated that if the variance of the bubbles' momenta is sufficiently large, the spatially homogeneous solution is stable and a phenomenon similar to Landau damping occurs. On the other hand, if the variance is too small the spatially homogeneous solution is unstable and the initial value problem is ill-posed. We demonstrate that the "damping" does not come from a stable eigenvalue, but instead, is associated with a resonance pole of the resolvent of the linearized evolution operator. The ill-posedness, on the other hand, is the result of an unstable eigenvalue. Numerical simulations are in complete agreement with the linear analysis and suggest that the long-time behavior in the ill-posed case results in bubble clustering. Our results are in agreement with those of Sangani & Didwania [12] and Smereka [13] and provide further insight into the results contained in these papers. Furthermore, the results of this paper suggest that the variance of the bubbles' momenta is a crucial quantity that should play an important role in developing effective equations for bubbly flow.

Acknowledgments

We express our gratitude to B. Brown for reading over this manuscript and thank Russel Caflisch for several helpful and fruitful discussions. We also thank Bill Lawson for pointing out Landau's work to us. We are grateful to Mario Pulvirenti for significant contributions in the derivation of the results of Appendix A.

Appendix A

We start from equations (36) and (38) with $u^\alpha = u_1^\alpha$, $p^\alpha = p_1^\alpha$, $x = x_1$ and $y = x_2$:

$$\rho_\ell u^\alpha = \frac{2}{\tau} p^\alpha - 9 J^\alpha,$$

$$J^\alpha_{mean}(x) = -\lim_{\epsilon \to 0} \frac{1}{4\pi} \int_{|x-y|>\epsilon} \frac{\partial^2}{\partial x^\alpha \partial x^\beta} \frac{j^\beta(y)}{|x-y|}\, dy,$$

and let

$$\tilde{J}^\alpha(x) \equiv -\frac{1}{4\pi} \frac{\partial^2}{\partial x^\alpha \partial x^\beta} \int \frac{j^\beta(y)}{|x-y|}\, dy.$$

Here the dependence on time is not explicitly indicated since it is not relevant. We prove the following:

Lemma 1

$$J^\alpha(x) = \tilde{J}^\alpha(x) - \frac{1}{3} j^\alpha(x)$$

Proof

$$\begin{aligned} \tilde{J}^\alpha(x) &= -\frac{1}{4\pi} \frac{\partial^2}{\partial x^\alpha \partial x^\beta} \int \frac{j^\beta(y)}{|x-y|}\, dy \\ &= -\frac{1}{4\pi} \frac{\partial}{\partial x^\alpha} \int \frac{\partial}{\partial x^\beta} \frac{j^\beta(y)}{|x-y|}\, dy. \end{aligned}$$

The last equality is correct because the integrands have a singularity which is integrable. We make use of the relation

$$\frac{\partial}{\partial x^\alpha} \frac{1}{|x-y|} = -\frac{\partial}{\partial y^\alpha} \frac{1}{|x-y|},$$

and obtain

$$\begin{aligned}\tilde{J}^\alpha(x) &= \frac{1}{4\pi}\frac{\partial}{\partial x^\alpha}\int\left(\frac{\partial}{\partial y^\beta}\frac{1}{|x-y|}\right)j^\beta(y)\,dy \\ &= \frac{1}{4\pi}\frac{\partial}{\partial x^\alpha}\left(\int\frac{\partial}{\partial y^\beta}\left(\frac{j^\beta(y)}{|x-y|}\right)dy - \int\frac{1}{|x-y|}\frac{\partial j^\beta}{\partial y^\beta}\,dy\right).\end{aligned}$$

The first integral in parenthesis vanishes, provided $|yj^\beta(y)| \to 0$ as $y \to \infty$, therefore

$$\begin{aligned}\tilde{J}^\alpha(x) &= -\frac{1}{4\pi}\frac{\partial}{\partial x^\alpha}\int\frac{1}{|x-y|}\frac{\partial j^\beta}{\partial y^\beta}\,dy \\ &= -\frac{1}{4\pi}\int\frac{\partial}{\partial x^\alpha}\frac{1}{|x-y|}\frac{\partial j^\beta}{\partial y^\beta}\,dy \\ &= \frac{1}{4\pi}\int\left(\frac{\partial}{\partial y^\alpha}\frac{1}{|x-y|}\right)\frac{\partial j^\beta}{\partial y^\beta}\,dy \\ &= \lim_{\epsilon\to 0}\frac{1}{4\pi}\int_{|x-y|>\epsilon}\left(\frac{\partial}{\partial y^\alpha}\frac{1}{|x-y|}\right)\frac{\partial j^\beta}{\partial y^\beta}\,dy \\ &= \lim_{\epsilon\to 0} I^\alpha_\epsilon(x) + J^\alpha_{mean}(x), \qquad (72)\end{aligned}$$

where

$$I^\alpha_\epsilon(x) \equiv \frac{1}{4\pi}\int_{|x-y|>\epsilon}\frac{\partial}{\partial y^\beta}\left(j^\beta(y)\frac{\partial}{\partial y^\alpha}\frac{1}{|x-y|}\right).$$

The integral $I^\alpha_\epsilon(x)$ can be computed using the divergence theorem,

$$I^\alpha_\epsilon = -\frac{1}{4\pi}\int_{|x-y|=\epsilon} j^\beta(y)\frac{\partial}{\partial y^\alpha}\frac{1}{|x-y|}n_\beta\,ds,$$

where n_β is the normal directed *out* of the ball $|x-y|<\epsilon$. We obtain

$$\begin{aligned}\lim_{\epsilon\to 0} I^\alpha_\epsilon &= \frac{1}{4\pi}j^\beta(x)\int_{|x-y|=\epsilon}\frac{y^\alpha - x^\alpha}{|x-y|}n_\beta\frac{ds}{|x-y|^2} \qquad (73)\\ &= \frac{1}{4\pi}j^\beta(x)\int_{|\xi|=1}\xi^\alpha\xi_\beta\,d\Omega = \frac{1}{3}j^\alpha(x), \qquad (74)\end{aligned}$$

as $\int_{|\xi|=1}\xi^\alpha\xi_\beta\,d\Omega = 0$ if $\alpha=\beta$ and

$$\int_{|\xi|=1}\xi^1\xi_1\,d\Omega = \frac{1}{3}\int_{|\xi|=1}\xi^\alpha\xi_\alpha\,d\Omega = \frac{4}{3}\pi. \qquad (75)$$

From (72) and (74) the proof of Lemma 1 follows. Q.E.D.

Making use of Lemma 1, one also has

$$\rho_\ell u^\alpha = \frac{2}{\tau} p^\alpha - 9\left(\tilde{J}^\alpha(x) - \frac{1}{3} j^\alpha(x)\right),$$

$$\tilde{J}^\alpha(x) = \frac{\partial \Phi}{\partial x^\alpha}, \qquad \text{and} \qquad \Delta\Phi = \nabla \cdot \vec{j}.$$

In one dimension it follows that $\tilde{J} = j$, therefore

$$\rho_\ell u = \frac{2}{\tau} p - 6j(x).$$

Appendix B

Here we prove the theorem stated in Sec. 5.

Theorem. *The equation $\mathcal{H}(\lambda; \varepsilon_0, \sigma) = 0$ with $\varepsilon_0 < 1/3$, has only one root with $Im(\lambda) > 0$ when $\sigma < \sigma_L(\varepsilon_0)$ and has no root with $Im(\lambda) > 0$ when $\sigma > \sigma_L(\varepsilon_0)$.*

There are four steps in the proof. First, we show that $H(\lambda; \varepsilon_0, \sigma)$ is an upper analytic function of λ. Next we see that for $\sigma = 0$ there is only one root with $\mathrm{Im}(\lambda) > 0$. This means that as σ is increased, roots can appear in the upper half-plane only by crossing the real axis from below. Nevertheless, the result of Section 5 shows that this can only happen at $\lambda = 1$ for $\sigma = \sigma_L(\varepsilon_0)$. Then, we prove that

$$\left.\frac{d\lambda_I}{d\sigma}\right|_{\lambda=1} < 0,$$

which shows that no roots come from the lower half plane as σ is decreased. We begin the proof with two lemmas.

Lemma 2.1. *$H(\lambda)$ is upper analytic in λ, with only one zero for $\sigma = 0$.*

Proof. Integrating by parts, we write Eq. (58) as

$$\mathcal{H}(\lambda) = 1 - \frac{3\varepsilon_0}{\sigma} \int \frac{p(p-2\lambda)}{(p-\lambda)^2} g\left(\frac{p-1}{\sigma}\right) dp.$$

Since $\lambda_I > 0$, the integration is performed along the real axis. With the substitution, $p = 1 + \sigma\xi$, the last equation can be written as follows:

$$\mathcal{H}(\lambda; \varepsilon_0, \sigma) = 1 - 3\varepsilon_0 \int_{-\infty}^{+\infty} \frac{(1+\sigma\xi)(1+\sigma\xi-2\lambda)}{(1+\sigma\xi-\lambda)^2} g(\xi)\, d\xi,$$

where, as before, the integration is along the real axis. The integrand is analytic for all real ξ, σ, and for Im $\lambda > 0$; the integral is finite for real σ and Im $\lambda > 0$. Therefore, $\mathcal{H}(\lambda; \varepsilon_0, \sigma)$ is then an analytic function for Im $\lambda > 0$. With $\sigma = 0$, the above equation becomes

$$\mathcal{H}(\lambda; \varepsilon_0, 0) = 1 - 3\varepsilon_0 \frac{1-2\lambda}{(1-\lambda)^2},$$

which has only one solution in the upper-half plane, when $\varepsilon_0 < 1/3$, namely,

$$\lambda = 1 - 3\varepsilon_0 + i\sqrt{3\varepsilon_0(1-3\varepsilon_0)}.$$

Q.E.D.

Lemma 2.2.

$$\left.\frac{\partial Im\lambda}{\partial \sigma}\right|_{\lambda=1} < 0 \quad at \quad \sigma = \sigma_L(\varepsilon_0).$$

Proof. We fix ε_0 and consider $\mathcal{H}$ to be a function of σ and λ, therefore,

$$\frac{\partial \lambda}{\partial \sigma} = -\frac{\partial \mathcal{H}}{\partial \sigma} \Big/ \frac{\partial \mathcal{H}}{\partial \lambda}. \tag{76}$$

Computations similar to those in Section 5 show that

$$\begin{aligned} \left.\frac{\partial \mathcal{H}}{\partial \sigma}\right|_{\lambda=1} &= 3\int \frac{p^2}{p-1}\frac{\partial^2 f_0}{\partial p \partial \sigma} dp \\ &= \frac{6\varepsilon_0 I}{\sigma^3} > 0, \end{aligned} \tag{77}$$

where I is given by (65) and

$$\mathcal{H}_\lambda \equiv \frac{\partial \mathcal{H}}{\partial \lambda} = 3\int \frac{p^2}{(p-\lambda)^2}\frac{\partial f_0}{\partial p} dp.$$

Writing $\lambda = \lambda_R + i\lambda_I$, we find

$$\mathrm{Im}(\mathcal{H}_\lambda) = -3\pi \int_{-\infty}^{+\infty} \frac{\partial D}{\partial p} p^2 \frac{\partial f_0}{\partial p} dp,$$

where

$$D \equiv \frac{\lambda_I}{\pi[(p-\lambda_R)^2 + \lambda_I^2]}.$$

Integrating by parts, we find that

$$\mathrm{Im}(\mathcal{H}_\lambda) = 3\pi \int D \frac{\partial}{\partial p}\left(p^2 \frac{\partial f_0}{\partial p}\right) dp.$$

Taking the limit as $\lambda_I \to 0$ and considering that $D \to \delta(p - \lambda_R)$, we obtain

$$\mathrm{Im}(\mathcal{H}_\lambda) = 3\pi \left.\frac{\partial^2 f_0}{\partial p^2}\right|_{p=1} < 0. \tag{78}$$

Lemma 2.2 follows when (78) and (77) are substituted into (76). Q.E.D.

Proof of the Theorem. From Lemma 2.1 it follows that there is only one root of $\mathcal{H}(\lambda) = 0$ for $\sigma = 0$. Since $\mathcal{H}$ is a continuous function of σ, the number of roots in the upper half plane can only change by roots crossing the real axis. In Sec. 5 we proved that when a root crosses the real axis, it does so at $\lambda = 1$ for $\sigma = \sigma_L(\varepsilon_0)$.

By Lemma 2.2 the root can only go from the upper-half plane into the lower-half plane as σ is increased. This means that for $\sigma < \sigma_L(\varepsilon_0)$, there is only one root in the upper-half plane. This root crosses the real axis at $\lambda = 1$ for $\sigma = \sigma_L(\varepsilon_0)$ and it remains in the lower-half plane for $\sigma > \sigma_L(\varepsilon_0)$. Q.E.D.

Appendix C

In this appendix we examine the spectrum of the linearized evolution operator and discuss the relationship of Landau damping to resonance poles. Much of this appendix is motivated by the work of Pego & Weinstein [40].

To begin, we take the Fourier transform of (54) to obtain

$$\frac{\partial \hat{f}_1}{\partial t} = \mathcal{L}\hat{f}_1 \tag{79}$$

where

$$\mathcal{L}\hat{f}_1(k,p,t) = ik(3j_0 - p)\hat{f}_1(k,p,t) - 3ikp\frac{\partial f_0(p)}{\partial p}\int_{-\infty}^{+\infty} q\hat{f}_1(k,q,t)\,dq. \tag{80}$$

We fix $k \neq 0$ and consider $\mathcal{L}$ to be an operator on $L^2(\mathbb{R})$. We then let μ be an eigenvalue of $\mathcal{L}$, i.e.

$$\mathcal{L}\hat{f}_1 = \mu\hat{f}_1. \tag{81}$$

The essential spectrum of $\mathcal{L}$ is the imaginary axis; since for $|p|$ large, $\mathcal{L}$ is dominated by ikp (see Crawford & Hislop [41]). To determine the point spectrum, we perform manipulations, similar to those used to arrive at Eq. (57), on (81) and obtain

$$\Lambda(\mu)\hat{j}_1 = 0, \tag{82}$$

where

$$\Lambda(\mu) = 1 + 3\int_{-\infty}^{+\infty} \frac{p^2}{p - 3j_0 - \frac{i\mu}{k}} \frac{\partial f_0}{\partial p} dp. \tag{83}$$

If we set $i\mu/k + 3j_0 = \lambda$ then (83) it is identical to (58) except for one important difference: the integration in (83) is always along the real axis. It follows from (82) that μ is an eigenvalue of $\mathcal{L}$ if

$$\Lambda(\mu) = 0. \tag{84}$$

It also follows that if $\mu = \mu_R + i\mu_I$ is a zero of $\Lambda(\mu)$ so is $\mu = -\mu_R + i\mu_I$. Combining this result with the results contained in Sec. 5, we can conclude that if $\sigma > \sigma_L$ the spectrum of $\mathcal{L}$ is the imaginary axis, and if $\sigma < \sigma_L$ a pair of eigenvalues appear, one stable and the other unstable. It is easy to verify that the eigenfunction for the eigenvalue, μ, is

$$\psi(p) = \frac{p}{p - 3j_0 - \frac{i\mu}{k}} \frac{\partial f_0}{\partial p}.$$

The above calculation shows that Landau damping cannot be associated with an eigenvalue of negative real part. In fact, the spectrum of $\mathcal{L}$ is entirely on the imaginary axis when Landau damping occurs. It turns out that the damping is a result of a resonance pole. In order to observe this, it is useful to introduce the resolvent of $\mathcal{L}$, which is defined as

$$\mathcal{R}_\mu = (\mathcal{L} - \mu)^{-1}. \tag{85}$$

In the stable case, $\sigma > \sigma_L$, this operator is well-defined and continuous for $\mathrm{Im}(\mu) \neq 0$. The resolvent is not continuous when $\mathrm{Im}(\mu) = 0$ (see, for example, Kolmogorov & Fomin [42]). This is because the spectrum is only on the imaginary axis in the stable case. If $\mathcal{R}_\mu$ is analytically continued across the essential spectrum of $\mathcal{L}$ (the imaginary axis) from the right-half plane, a pole is formed in the left half plane and is called a resonance pole.

This resonance pole is responsible for the Landau damping. As the σ is lowered past σ_L, the resonance pole crosses the imaginary axis and becomes the unstable eigenvalue. A similar construction can be used to understand the emergence of the stable eigenvalue, (see Pego & Weinstein [40], for more details).

Let us construct this argument explicitly. We can rewrite Eq.(55) as

$$sF_1 - \hat{f}_1(k,p,0) = \mathcal{L}F_1$$

which can easily be cast in the following form:

$$J_1 = -\int_{-\infty}^{+\infty} \mathcal{R}_s(\hat{f}_1(k,p,0))p\,dp \tag{86}$$

where the resolvent has been analytically continued in the manner suggested by Landau and as described in Figure 1. It was found in Sec. 5 that when σ was lowered past σ_L, the poles of J_1 moved from the right-hand side of the complex s-plane to the left-hand side. Therefore, we see that the poles that occur in $\mathcal{R}_s$ when $\sigma > \sigma_L$ are responsible for the Landau damping. Crawford & Hislop [41] present a somewhat different approach.

References

[1] G.B. Wallis, "Interial coupling in two-phase flow: Macroscopic properties of suspensions in an inviscid fluid", *Multiphase Science and Technology*, **5**, 239 (1989).

[2] L. van Wijngaarden," Geurst's stability criterion for concentration waves in bubbly fluids ", *Int. J. Multiphase Flow*, **17**, 809 (1991).

[3] J. A. Geurst, " Virtual mass and impulse of bubble dispersions: reply to a note by van Wijngaarden", *Int. J. Multiphase Flow*, **17**, 815 (1991).

[4] A. Biesheuvel and L. van Wijngaarden, "Two phase flow equations for a dilute dispersion of bubbles", *J. Fluid Mech.*, **148**, 301 (1984).

[5] D.A. Drew and R.T. Wood, "Overview and Taxonaomy of Models and Methods" , Workshop on Two-Phase Flow Fundamentals, National Bureau of Standards, Maryland, September 1985.

[6] D. Lhuillier,"Phenomenology of interia effects in a dispersed solid-fluid mixture", *Int. J. Multiphase Flow*, **11**, 427 (1985).

[7] C. Pauchon and S. Banerjee " Interphase momentum interaction effects in the averaged multifield model. Part I: void wave propagation in bubbly flows", *Int. J. Multiphase Flow*, **12**, 559 (1986).

[8] P. van Beek, "$O(\alpha)$- accurate modeling of the virtual mass effects in a liquid-bubble dispersion", *App. Sci. Res.*, **38**, 323 (1982).

[9] J. A. Geurst, "Virtual mass effects in two-phase flow", *Physica*, **129A**, 239 (1985).

[10] C. Pauchon and P. Smereka,"Momentum interactions in dispersed flow: An averaging and a variational approach", *Int. J. Multiphase Flow*, **18**, 65 (1991).

[11] P. Smereka and G. W. Milton, "Bubbly Flow and its relation to conduction in composites", *J. Fluid Mech.*, **233**, 65 (1991).

[12] A. S. Sangani and A.K. Didwania, " Dynamic simulations of flows of bubbly liquids at large Reynolds numbers", *J. Fluid Mech.* 1993, to appear.

[13] P. Smereka, "On the dynamics of bubbles in a periodic box", *J. Fluid Mech.*, to appear.

[14] A. Biesheuvel and W.C.M. Gorissen, "Void fraction disturbances in a uniform bubbly liquid", *Int. J. Multiphase Flow*, **16**, 211 (1990).

[15] L. van Wijngaarden and C. Kapteyn "Concentration waves in dilute bubble/liquid mixtures", *J. Fluid Mech.*, **212**, 111 (1990).

[16] G.K. Batchelor,"A new theory of the instability of a uniform fluidized bed", *J. Fluid Mech.*, **193**, 75 (1988).

[17] L. Landau," On the vibrations of the electronic plasma" *J. Physics (U.S.S.R.)*, **10**, 25 (1946).

[18] A. S. Sangani and A.K. Didwania, "Dispersed phase stress tensor of bubbly liquids at large Reynolds numbers", *J. Fluid Mech.*, 1993, to appear.

[19] C. Jacoboni and P. Lugli, "The Monte Carlo Method for Semiconductor Device Simulation", Springer-Verlag, 1969.

[20] H. Lamb, "Hydrodynamics", 6th ed. Cambridge University Press 1932 (Dover edition 1945).

[21] A. B. Basset, "On the motion of two spheres in a liquid", *Proc. Lond. Math. Soc.*, **18**, 369 (1887)

[22] H. S. Kim and A. Prosperetti, "Numerical simulation of the motion of rigid spheres in potential flow", *SIAM J. Appl. Math.*, **526**, 1533–1562 (1992).

[23] S. Chapman and T.G. Cowling, "The mathematical theory of non-uniform gases", Cambridge University Press, Cambridge, 1970.

[24] R.L. Liboff, "Introduction to the theory of kinetic equations", Wiley, New York, 1969.

[25] G. Sandri, "The foundations of nonequilibrium statistical mechanics, I" *Ann. of Phys.*, **24**, 394 (1963).

[26] J.R. Rietz and F.J. Milford, "Foundations of electromagnetic theory", Addison-Wesley, London, 1960.

[27] G.A. Bird "Molecular Gas Dynamics", Claredon Press, Oxford, 1976.

[28] H. Neunzert, "An introduction to the nonlinear Boltzmann-Vlasov equation", in "Kinetic Theory and the Boltzmann Equation", *Lecture Notes in Mathematics*, **1048**, 60–110 (1984).

[29] A.A. Vlasov, "Many particle theory and its application to plasma", Gordon and Breach , New York, 1961.

[30] R.L. Liboff, "Kinetic approach to condensation", *Physical Review*, **131**, 2318 (1963).

[31] S.G. Chefranov, "Dynamics of point vortex dipoles and spontaneous singularities in three dimensional turnulent flows", *Sov. Phys. JETP*, **66**, 85 (1987).

[32] Yu.N. Grigoryev and N.N. Yanenko, "Hamiltonian vortex models in the theory of turbulence", *Archives on Mechanics*, **345**-6, 621-631 (1982).

[33] V.I. Oseledets, "On a new way of writing the Navier-Stokes equation: The Hamiltonian formalism", *Russ. Math. Surveys*, **44**, 210 (1989).

[34] T.F. Buttke "Lagrangian numerical methods which preserve the Hamiltonian structure of incompressible fluid flow", preprint (1993).

[35] R.W. Hockney and J.W. Eastwood, "Computer Simulation Using Particles", McGraw-Hill, New York, 1981.

[36] C.K. Birdsall and A.B. Langdon, "Plasma Physics via Computer Simulation", McGraw-Hill, 1985.

[37] P. Billingsley, "Convergence of Probability Measures", J. Wiley and Sons, New York, 1968.

[38] L. Kuipers and H. Niederreiter, "Uniform Distribution of Sequences", Wiley, New York, 1974.

[39] G.K. Batchelor, " An introduction to fluid dynamics", Cambridge University Press, New York, 1990.

[40] R.L. Pego and M.I. Weinstein, "Eigenvalues and instabilities of solitary waves",*Phil. Trans. R. Soc. Lond. A*, **340**, 47 (1992).

[41] J.D. Crawford and P.D. Hislop "Application of the method of spectral deformation to the Vlasov-Poisson system. II. mathematical results", *J. Math. Phys.*, **30**, 2819 (1989)

[42] A.N. Kolmogorov and S.V. Fomin, "Introductory Real Analysis", Dover, New York, 1975.

Figure Captions

Figure 1 Integration path in the complex plane that is used to define $\mathcal{H}(\lambda)$.

Figure 2 Location of the points in phase space for the case $\varepsilon_0 = 0.01, \sigma = 0.5$ and $\alpha = 0.6$. The parameters used in the computation are $L = 100, N_c = 20$, and $N = 65,535$; the time step is $\Delta t = 0.1$. We have only plotted 2,000 points randomly selected from the 65,535 points used in the computation. Figure (a) is at $t = 0$ and the subsequent figures are at time intervals of 80.

Figure 3 This shows the momentum flux, $j(x,t)$, for the same times as in Figure 2. The circles are the result of the particle code and the continuous line represents the exact solution of the linearized equations.

Figure 4 Location of points in phase space for the case $\varepsilon_0 = 0.01, \sigma = 0.2$ and $\alpha = 0.1$. The numerical parameters are the same as those given in Figure 2.

Figure 5 This shows the momentum flux, $j(x,t)$, for the same times as in Figure 4. The circles are the result of the particle code and the continuous lines represent the exact solution of the linearized equations.

Figure 6 Location of points in phase space for the case $\varepsilon_0 = 0.01, \sigma = 0.1$ and $\alpha = 0.4$. The numerical parameters are the same as those given in Figure 2 and the time interval between successive pictures is 320. This case shows the clustering of the bubbles in space.

Figure 7 This shows the momentum flux, $j(x,t)$, for the same times as those in Figure 6. The clustering is shown by the spike in $j(x,t)$.

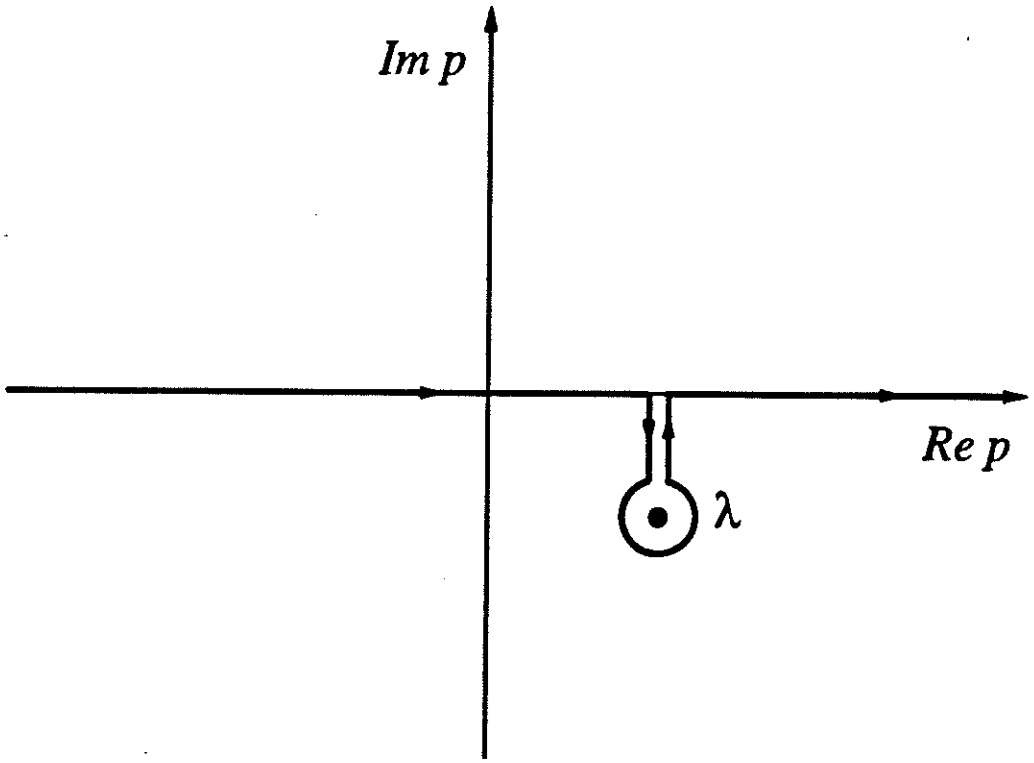

Figure 1
Russo & Smereka I

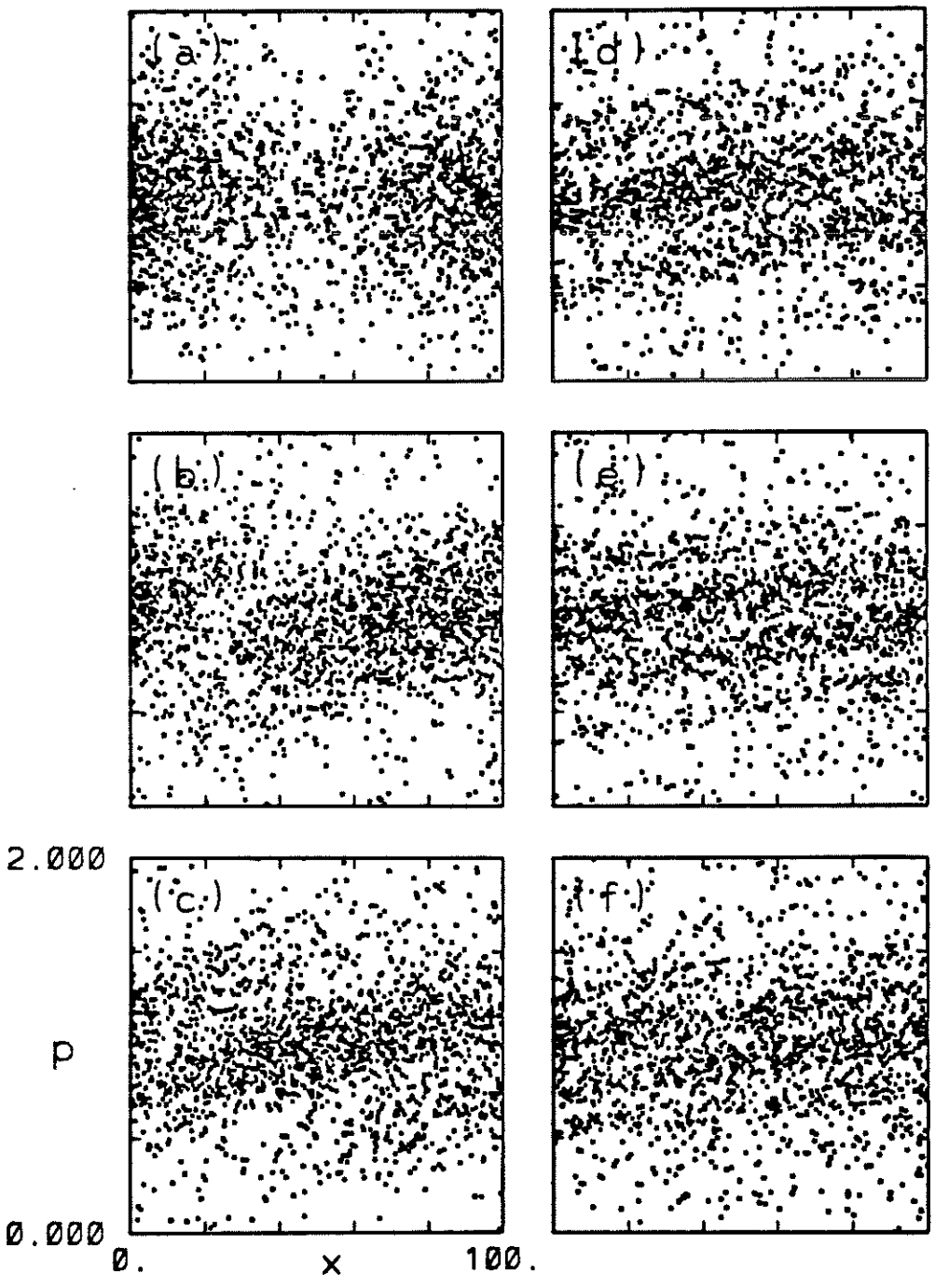

Figure 2
Russo & Smereka I

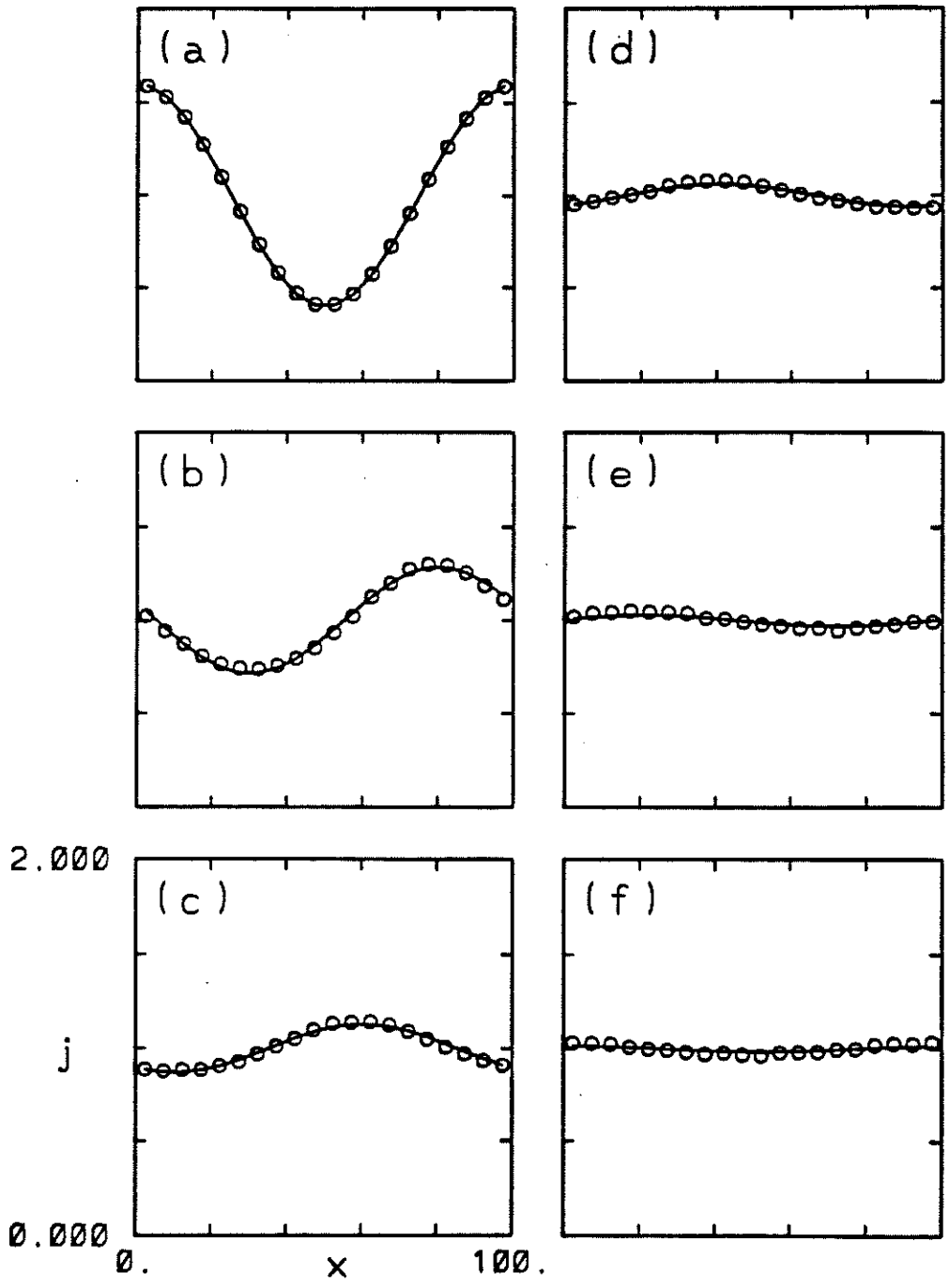

Figure 3
Russo & Smereka I

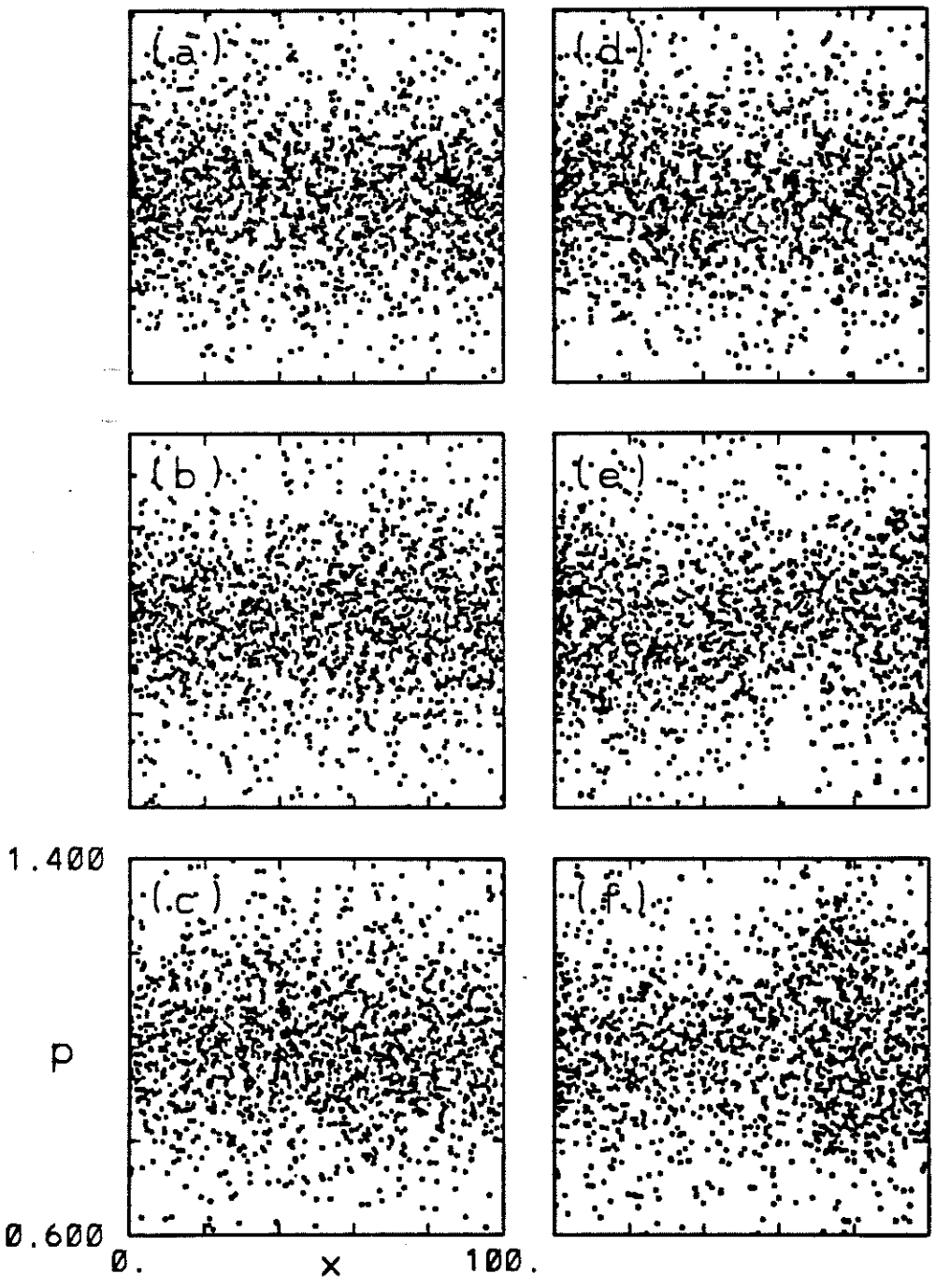

Figure 4
Russo & Smereka I

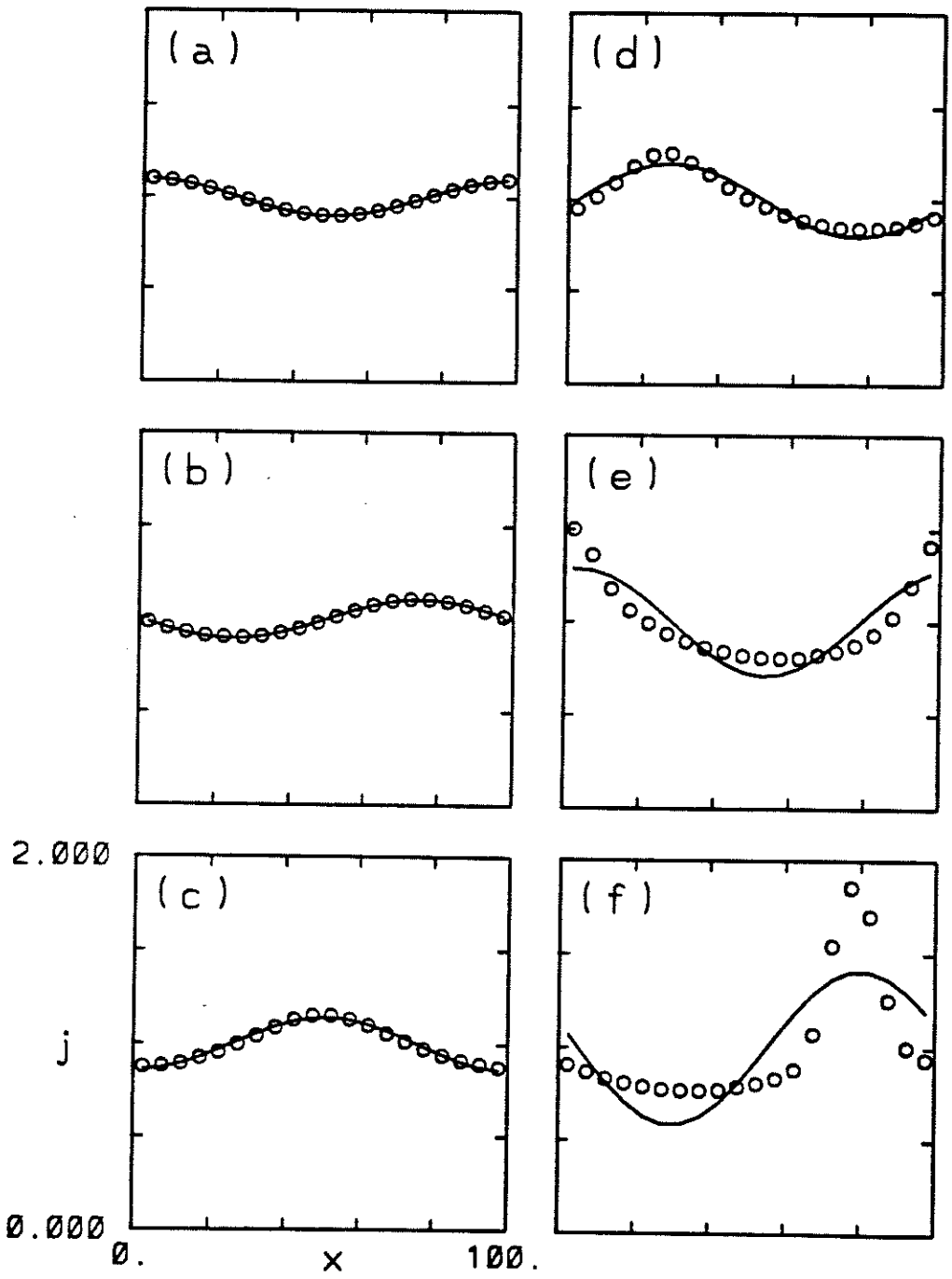

Figure 5
Russo & Smereka I

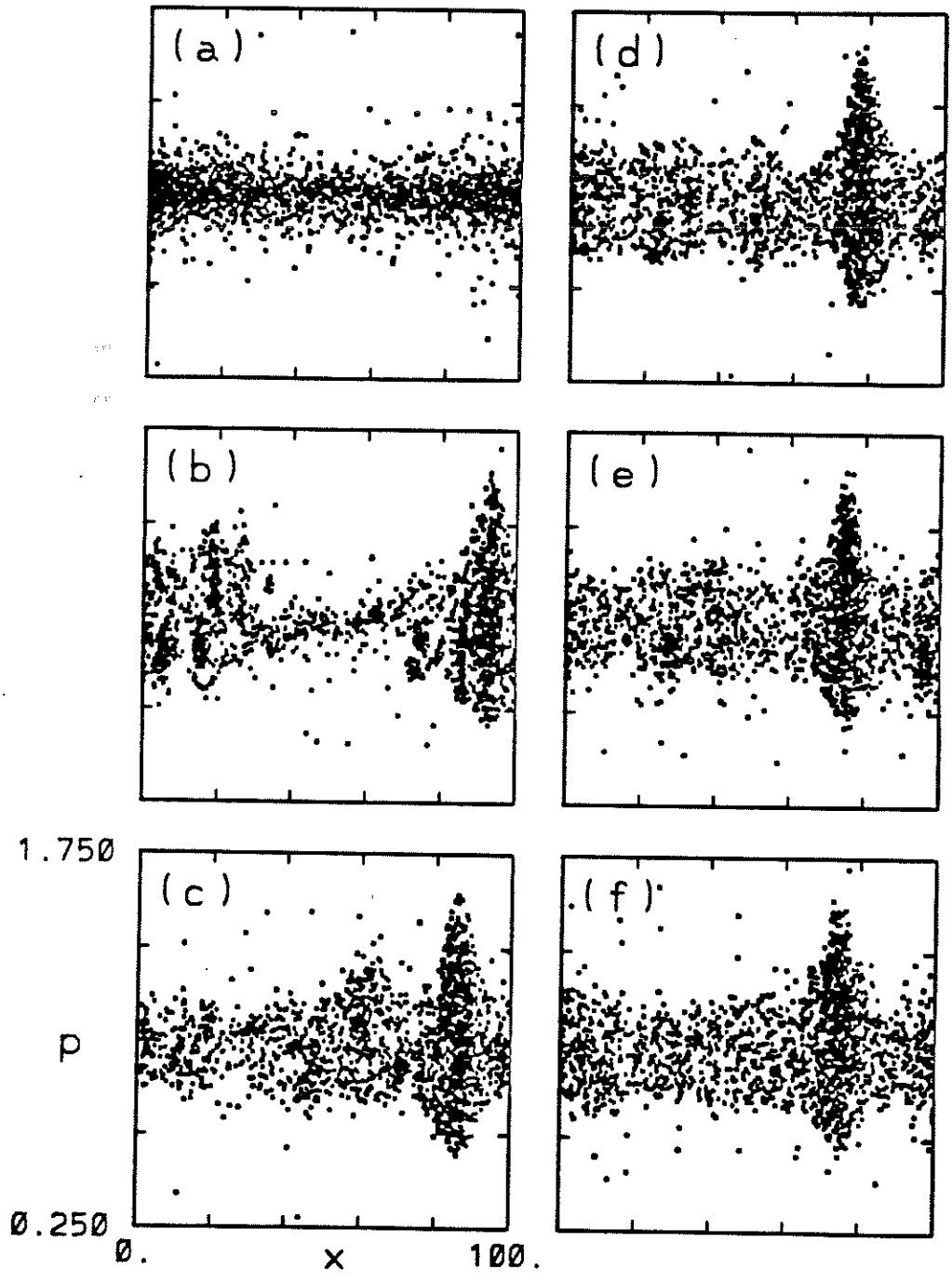

Figure 6
Russo & Smereka I

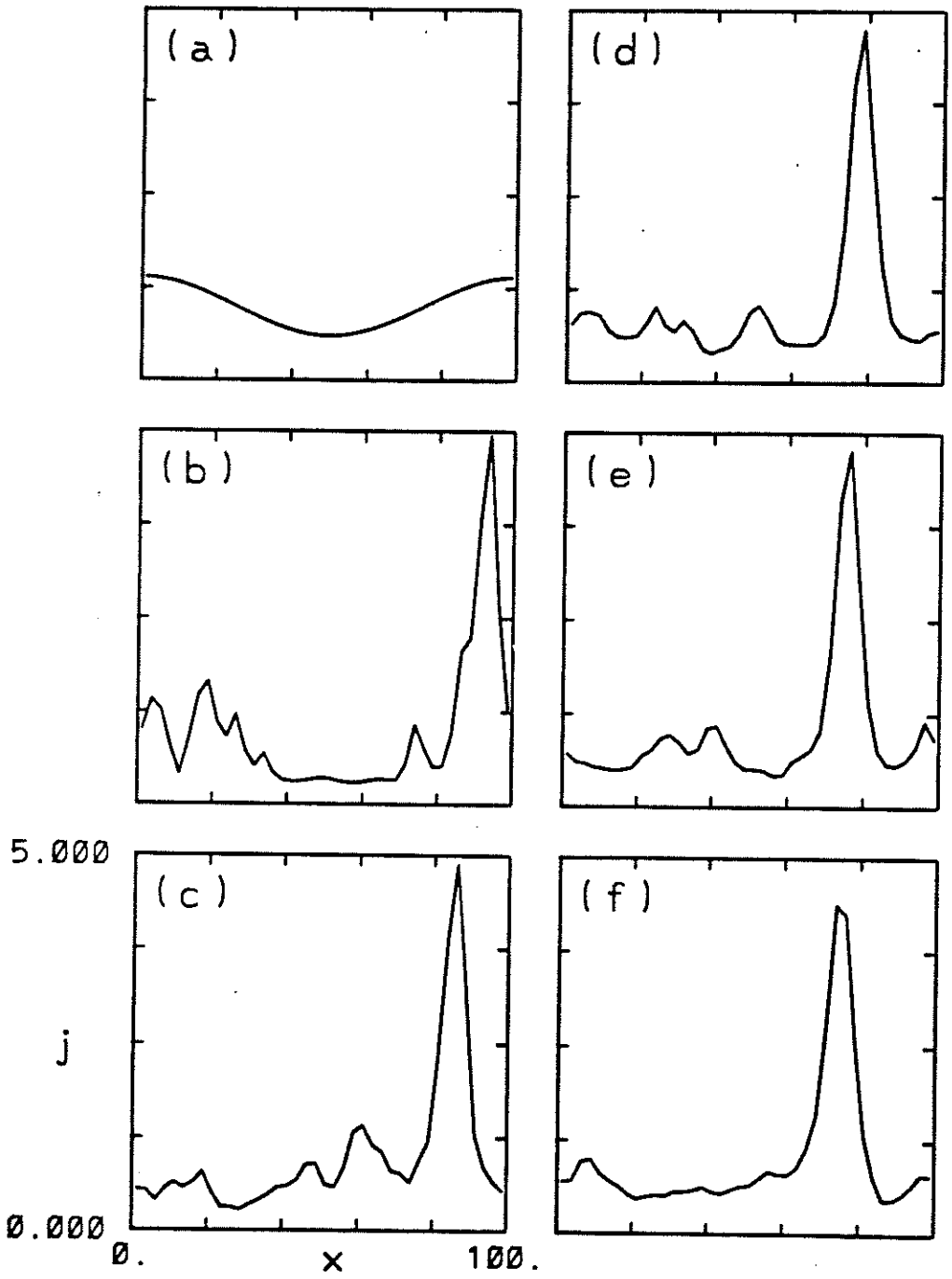

Figure 7
Russo & Smereka